Polar aerosol rivers: detection, characteristics and potential applications

Rémy Lapere[1], Jennie L. Thomas[1], Vincent Favier[1], Hélène Angot[1], Julia Asplund[2,3], Annica M. L. Ekman[2,4], Louis Marelle[5], Jean-Christophe Raut[5], Anderson Da Silva[5], Jonathan D. Wille[6], Paul Zieger[2,3]

[1]Univ. Grenoble Alpes, CNRS, IRD, Grenoble INP, IGE, 38000 Grenoble, France
[2]Bolin Center for Climate Research, Stockholm, Sweden
[3]Department of Environmental Science, Stockholm University, Stockholm, Sweden
[4]Department of Meteorology, Stockholm University, Stockholm, Sweden
[5]LATMOS/IPSL, Sorbonne Université, UVSQ, CNRS, Paris, France
[6]Institute for Atmospheric and Climate Science, ETH Zurich, Zurich, Switzerland

Key Points:

- A catalog of polar aerosol rivers (AeR) is provided for 1980–2022 by adapting an atmospheric river (AR) detection scheme
- Important AeR events, representing rapid poleward transport of aerosol-enriched air masses, are presented
- Combining AR and AeR can improve our understanding of the links between mid- and polar-latitudes, in the past, present and future climate

Corresponding author: Rémy Lapere, `remy.lapere@univ-grenoble-alpes.fr`

Abstract

Aerosols play a key role in polar climate, and are affected by long-range transport from the mid-latitudes, both in the Arctic and Antarctic. This work investigates poleward extreme transport events of aerosols, referred to as aerosol rivers (AeR), leveraging the concept of atmospheric rivers (AR) which signal extreme transport of moisture. Using reanalysis data, we build a detection catalog of polar AeRs for black carbon, dust, sea salt and organic carbon aerosols, for the period 1980–2022. First, we describe the detection algorithm, discuss its sensitivity, and evaluate its validity. Then, we present several extreme transport case studies, in the Arctic and in the Antarctic, illustrating the complementarity between ARs and AeRs. Despite similarities in transport pathways during co-occurring AR/AeR events, vertical profiles differ depending on the species, and large-scale transport patterns show that moisture and aerosols do not necessarily originate from the same areas. The complementarity between AR and AeR is also evidenced by their long-term characteristics in terms of spatial distribution, seasonality and trends. AeR detection, as a complement to AR, can have several important applications for better understanding polar climate and its connections to the mid-latitudes.

Plain Language Summary

The extreme transport of aerosol-containing air masses, from the mid-latitudes to the polar regions, can be characterised and quantified by leveraging Aerosol Rivers (AeRs). This is similar to the Atmospheric Rivers (ARs) which carry large amounts of water to the poles and affect the overall stability of polar ecosystems. In this work, we establish a detection algorithm for AeRs and evaluate it for different well-known aerosol intrusions or AR events. The areas most affected by AeRs are described, their trends are investigated and we discuss the potential applications of AeR detection for a better understanding of polar climate.

1 Introduction

Aerosols and clouds (and their interactions) are of particular concern because they comprise a large uncertainty in global climate predictions, including in the Arctic and Antarctic (Myhre et al., 2013; Szopa et al., 2021), as well as the fact that the polar regions are experiencing climate change more than any other region of the planet (Hall, 2004; Rantanen et al., 2022). This faster change is also impacted by the cloud phase feedback, which is influenced by aerosols (Tan & Storelvmo, 2019). In addition, the polar regions are largely snow and ice covered and one important polar climate feedback mechanism is through deposition of light absorbing aerosols (including dust and black carbon) which darkens these surfaces and accelerates melting/warming (Bond et al., 2013; Skiles et al., 2018). Therefore, it is critical to be able to estimate the aerosol budget in the polar regions, including from rapid transport from the mid-latitudes towards the poles (Schmale et al., 2021).

The aerosol lifecycle in the polar regions has particular characteristics compared to typical urban or remote regions found at mid-latitudes. Primary aerosol sources are limited in the Arctic and Antarctic, and include sea spray (Abbatt et al., 2019; Kirpes et al., 2019; Frey et al., 2020) as well as local dust from ice-free terrain (Bullard et al., 2016; Amino et al., 2021; Meinander et al., 2022), and limited local anthropogenic sources (Marelle et al., 2018). As a result, intrusions of aerosol-containing mid-latitude air masses contribute significantly to the aerosol budget in the Arctic (J. L. Thomas et al., 2017; Zhao et al., 2022) and Antarctic (Jumelet et al., 2020), and may affect polar cloud properties with important climate implications (Dada et al., 2022; Shi et al., 2022). In the Arctic in winter and spring, the polar dome expands to include some parts of Europe, Eurasia, and North America, so that pollution from the mid-latitudes can be transported at low levels towards the Arctic, which is known as the Arctic Haze phenomenon (Barrie, 1986; Quinn et al., 2007). Aerosols are also transported from lower latitudes into the Arctic dome via three possible pathways: low-level transport followed by uplift upon reaching the dome and eventually descent, direct injection into the free troposphere at the source followed by long-range transport, or via mid-latitude cyclones transporting pollutants in the free troposphere into the Arctic (Stohl, 2006; M. A. Thomas et al., 2019). Several of these circulation types can be associated with warm air mass intrusions, as reviewed in Pithan et al. (2018), or the more extreme atmospheric rivers (AR), which also bring large quantities of moisture and precipitation to the polar regions (Gorodetskaya et al., 2014; Turner et al., 2019; Maclennan & Lenaerts, 2021).

ARs are defined as long filamentary bands of poleward moisture transport often embedded within the low-level jet ahead of an extratropical cyclone's cold front. They make a major contribution (90%) to the transport of water vapor from the interior of the tropics to the mid-latitudes and the poles, even though they cover only about 10% of the surface area; four or five AR in each hemisphere may therefore be sufficient to carry the majority of meridional flows across the globe (Zhu & Newell, 1998; Nash et al., 2018). ARs are low-frequency, high-impact events with major implications for the global hydrological cycle. They have been linked with flooding and drought busting in the mid-latitudes (Lavers et al., 2012; Neiman et al., 2013; Ralph et al., 2019), and ice-sheet mass balance impacts in polar regions (Mattingly et al., 2018; Wille et al., 2019, 2021, 2022; Adusumilli et al., 2021). Due to their crucial role in the hydrological cycle, various global AR detection algorithms have been developed, as summarized for example in the Atmospheric River Tracking Method Intercomparison Project (ARTMIP) program (Shields et al., 2018, 2022). ARs in the mid-latitudes have been shown to initiate the deposition of long-range transport dust and biological aerosols through ice riming when the AR moisture is forced upward through orographic or isentropic ascent (Creamean et al., 2013; Francis et al., 2022).

Inspired by the concept of ARs, Chakraborty et al. (2021, 2022) proposed the definition of aerosol atmospheric rivers (AARs) to characterize the rapid, large-scale trans-

port of large quantities of aerosols. Chakraborty et al. (2021) developed an objective global algorithm to detect AARs and demonstrated that they play a crucial role in long-range transport pathways, accounting for a significant fraction (40–80%) of global total aerosol transport over relatively few events (20–40 AAR days/year). These works demonstrated that AARs can be detected and are useful for investigating and quantifying aerosol transport.

For polar applications, it is important to adapt the detection of AARs to the specific characteristics of poleward transport. This is similar to the case of ARs, where there is a large spread in AR detection frequency between global and regional methods (Collow et al., 2022). Due to the lower moisture capacity of colder, polar atmospheres, most global AR detection algorithms tend to capture an overly broad swath of extratropical cyclone activity instead of the more characteristically intense meridional moisture transport seen in ARs. Thus a regional detection method is better suited for studying AR connections with modes of variability, especially around the Southern Ocean (Shields et al., 2022).

Here, we follow the development of the concept of AARs, from Chakraborty et al. (2021, 2022), but adapt the polar AR detection method developed by Wille et al. (2019) to do so, in order to identify polar oriented extreme transport of aerosols. These will be referred to as aerosol rivers (AeR) hereafter (since aerosols are inherently in the atmosphere). Leveraging this detection, we aim to answer the following scientific questions:

- What are the characteristics and climatology of polar AeRs?
- How do polar AeRs compare with ARs?
- Can AeRs provide a moisture-independent characterization of atmospheric circulation during extreme poleward transport events?

In order to answer these questions, the paper is organized into the following sections. In Section 2, the algorithm and the input data used for AR and AeR detection are described. Then, we show case studies of major ARs and AeRs, validating the detection method and illustrating the interest of a combined approach to extreme transport events (Section 3). The climatology and characteristics of AeR in the Arctic and the Antarctic obtained with this algorithm are also presented in Section 3. Finally, we discuss the potential applications of this AeR catalog in Section 4.

2 Data and Methods

2.1 AR and AeR detection methods

The quantity of interest for AeR detection is the vertically integrated, meridional mass flux of aerosol (denoted vIxT), as described by Equation 1.

$$\mathrm{v}IxT = \int_{surface}^{top} V x \, dp \tag{1}$$

where V is the meridional wind speed, dp is the pressure level increment, and x is the transported quantity of interest (water vapor mixing ratio for AR, aerosol mixing ratio for AeR).

We focus on three key aerosol species for AeRs including: black carbon (BC), dust (DU), and sea-salt (SS). These three species are selected because they are representative of different types of emission sources and processes, and cover most of the global mass of primary aerosols (Chin et al., 2002). Organic Carbon (OC) AeRs are also considered for a case study although the climatology is not investigated in detail. For each time step, whenever a grid point has a vIxT directed poleward (i.e. positive for the Northern Hemisphere, negative for the Southern Hemisphere), and a value greater than the historical 97^{th} percentile (P97) of the corresponding month, over the 1980–2022 climatology, it is

considered an AeR-participating point. The choice of P97 is discussed in Section 3.1. When a continuous area (i.e. a contour) of AeR-participating points extends more than 20 ° in latitude, an AeR is detected. This detection scheme is adapted from Wille et al. (2019, 2021) and applied in this work both to integrated meridional fluxes of water vapor for the detection of ARs, and to integrated meridional fluxes of BC, DU, SS and OC for AeRs. The suitability of the 20 °-latitude extent criterion for AeR is discussed in Section A1. The validation of the adaptations compared to the original AR detection method is provided in Section A1.

The definition of an AR consists in selecting extreme events based on considerations of extreme moisture transport amounts. The detection algorithms take into account an AR event by analyzing points where the integrated vapor transport (IVT) exceeds a threshold value. For AR detection, the threshold is taken at P97 here, as it matches best with the reference AR climatologies from Wille et al. (2019), with the MERRA2 input data used here (described in Section 2.2), although Wille et al. (2019) used a P98 threshold instead. This is connected to different spatial resolutions and assumptions in the computation of IVT (different vertical extent for the integration), as explained in Section A1.

Like for AR, a key parameter for an AeR detection methodology is the threshold for which grid cells are considered AeR-participating. There is no reason why the same number of events should be found for different aerosols. The definition of an AR or AeR event should therefore be based solely on an objective and independent statistical detection criterion, regardless of the aerosol type under consideration. For this reason, we recommend considering the same percentile for all aerosol types. In this work, we chose to remain consistent between the transport of moisture and aerosols in order to capture similar types of anomalous events, regardless of the transported quantity. As a result, the threshold P97 is also used for AeRs.

The algorithms for AR and AeR detection described in this work are implemented in a Python3 Jupyter Notebook (Kluyver et al., 2016). This code leverages the contour detection offered by the Matplotlib library (Hunter, 2007), and the image analysis tools from the OpenCV library (Bradski, 2000) which provides an efficient way of masking 2-dimensional data. The corresponding detection catalogs for AR and AeR, based on MERRA2 vertically integrated fluxes at 1 ° x 1 ° spatial resolution (see Section 2.2) and covering the period 1980–2022, along with the processing and detection codes, are available at `https://doi.org/10.5281/zenodo.8082768` (Lapere, 2023).

2.2 MERRA2 data

The data used for AR detection is the MERRA2 hourly Vertically Integrated Diagnostics, *northward flux of atmospheric water vapor*. Similarly, the detection of AeRs is performed using the MERRA2 hourly Vertically Integrated Diagnostics, *dust/black carbon/sea salt/organic carbon column v-wind mass flux*. The MERRA2 aerosol product was also used in Chakraborty et al. (2021, 2022) for AAR detection. These products are integrated fluxes over the whole atmospheric column (1000 hPa to 0.1 hPa). Additionally, large scale meteorological conditions (500 hPa geopotential height, 500 hPa winds and surface precipitation) associated with the case studies presented are extracted from the single-level MERRA2 hourly reanalysis. Geopotential height anomalies are computed as the difference between the hourly values averaged over the considered event and the monthly mean climatology for the corresponding month. For these case studies, vertical profiles of aerosol and water mixing ratio are from the MERRA2 hourly product on pressure levels. Total column mass concentration and surface concentration of aerosols, as well as aerosol optical thickness are from the MERRA2 hourly single level aerosol assimilation product. All data sets are systematically re-gridded to the 1 °x1 ° spatial resolution and re-sampled to a 3-hourly time resolution. Monthly aerosol emission fluxes

from MERRA2 are also considered, for the 1980–2022 period. For readability, the references corresponding to these data sets are summarized as Global Modeling and Assimilation Office (GMAO) (2015a, 2015b, 2015c, 2015d, 2015e).

3 Results and discussion

3.1 Polar AeR detection thresholds

The sensitivity of the AeR detection to the threshold choice is tested in Figure 1a. With a P99 threshold, the fraction of grid points above 60 °N or below 60 °S which belong to an AeR is less than 0.2%, on average, for all aerosol species and both poles. With P97, this number increases at around 0.5–1% for non SS species. For SS this number is lower, at 0.2%. As the threshold decreases, the number of AeR points increases, up to around 20% of the domain, on average, for a P65 threshold. This illustrates how strongly the detection depends on the selection of the threshold.

In Figure 1b, we look at the percentage of AR points, over the climatology, which are also AeR points (i.e. overlapping contours), using different AeR detection thresholds (but keeping P97 for ARs). We investigate this sensitivity for BC, DU, SS and OC, for the Arctic and the Antarctic, with similar conclusions for all, irrespective of the hygroscopic nature of the aerosol type. For percentiles above P85, the slope is steep and the number of co-located AR and AeR points varies strongly, between less than 5% for P99, and up to 70% for P85. For percentiles below P85, the number of co-occurrences starts to reach its asymptotic value of 70-80%. This shows that no matter what percentile threshold is chosen for AeRs, 20% to 30% of AR grid cells cannot be described as AeR grid cells, and therefore belong to pristine (no aerosol) AR cases. This illustrates that while ARs and AeRs may be similar (see Section 3.3), they describe different phenomena.

Figure 1 also shows that SS AeRs behave differently from other AeR types. For similar detection thresholds, SS AeR are detected less often than for other aerosols, and also coincide less often with ARs. This can be connected to the relatively closer source of SS in polar regions compared to other aerosol sources. The DU and BC aerosols found at the poles mostly originate from the mid-latitudes, but SS is mainly emitted from open ocean areas, such as the Southern Ocean or North Atlantic and North Pacific, which are located closer to the poles. As a result, the background SS is higher and the regional transport more frequent, which leads to a higher P97 and therefore lower frequency of SS AeR. The implications of this result are further discussed in the continuation.

3.2 Validation of the detection with case studies

Here we study events of AR and large aerosol transport which were well monitored and documented in the literature, in order to assess if they are well captured by our detection algorithm. We analyze these case studies using both the AR and AeR detections and show the interest of adopting a combined analysis approach for a better understanding of extreme poleward transport events.

3.2.1 2013 Asian dust transport to the Arctic

A dust transport event from Asia to the high Arctic, originating from the Gobi desert, was recorded in March 2013, which resulted in several days of enhanced pollution measured at Arctic stations (Zhao et al., 2022). Although this event was originally studied from the point of view of dust transport, the AR/AeR detection scheme developed in this study shows that extreme transport of other aerosols and water vapor also occurred simultaneously at these dates, along the same pathways, with AR, BC AeR and SS AeR detected in addition to the DU AeR (Figure 2). Figure A1 reveals that the DU transport was originally zonal above Asia, and turns poleward near the 180 ° longitude mark,

where AR and AeRs are detected, extending from 35 °N to 90 °N. This spatial pattern is consistent with the findings from Zhao et al. (2022). Figure A1 also shows that although the AR/AeRs have similar spatial extents, they are associated with transport originating from different areas. DU comes from the Gobi desert, but BC comes from the industrial regions of southeast China, SS comes from the Pacific Ocean, and water vapor comes from the China sea and Pacific Ocean. Therefore, these similar AR/AeR detections actually connect different sources to the receptor region in the Arctic.

The vertical profiles associated with this transport event (Figure 2) reveal that the DU aerosols are transported in two layers, at around 700 hPa and 400 hPa. BC aerosols are found in the same 700 hPa layer, but not higher up in the atmosphere. In comparison, the SS aerosols and moisture along the transect are mostly found near the surface, below 800 hPa, in connection with more local sources of SS and moisture. The DU and BC transport pathway near 700 hPa is consistent with the transport mechanism from Asia due to lifting of air mass and slow descent in the Arctic due to radiative cooling, described in Stohl (2006). The 400 hPa secondary DU layer on the other hand can either come from longer range transport, or from the same source region and have been lifted higher up at another time, as illustrated by the back-trajectories in Roiger et al. (2011). This layer may also come from the generally excessive concentrations of DU in the polar free troposphere in MERRA2 (Böö et al., 2023).

This event was of importance for the Arctic climate: Zhao et al. (2022) estimate that it contributed to a reduction of snow and ice albedo of around 2%, due to deposition of dust and soot. Therefore, quantifying the frequency of such events is critical for a better understanding of the Arctic climate. Moreover, this Asian dust transport event was recorded as a polar crossing event (which is also illustrated by Figure A1), with increases in particulate matter concentration as far as Alert, Canada (Zhao et al., 2022). Therefore, we would expect the DU AeR contour to reach this region. However, the AeR detection is, by design, unable to capture polar crossing events since the condition for the detection of an AeR is that the transport has to be directed toward the pole. This is a limitation of the current algorithm, which is also a limitation of polar AR detection methods. Similar polar-crossing aerosol transport events were also observed and studied in Sodemann et al. (2011); Raut et al. (2017), for example, which justifies improving current algorithms for a more comprehensive detection.

3.2.2 2020 European pollution transport to the Arctic

In April 2020, an extreme aerosol transport event was recorded in the central Arctic (85 °N, 15 °E) during the international Multidisciplinary drifting Observatory for the Study of the Arctic Climate (MOSAiC) expedition (Shupe et al., 2022; Dada et al., 2022) which involved the Polarstern research vessel. Measurements showed strong, rapid increases in aerosol surface concentrations, including BC and OC. This event is well captured by our detection algorithm (Figure 3), with an AR detected on April 15, at the onset of the event, which was described as driven by a warm air mass intrusion by Dada et al. (2022). In parallel, a BC and an OC AeR are detected on the same day, lasting for 3 consecutive days, during which increased BC surface concentrations were recorded (Figure 3b). Dada et al. (2022) also noted increased concentrations of OC in addition to BC, with which our OC AeR detection is also consistent. Figure 3c further shows that MERRA2 captures this event adequately, with BC surface mixing ratios rising up to $0.3\,\mu g\,kg^{-1}$ both in the observations and the reanalysis at the location of the ship (orange square in Figure 3c).

The vertical profiles associated with this event reveal that the transport of aerosols occurs at several altitudes (Figure 3c). The large quantities of BC and OC close to the surface are consistent with the observations from Dada et al. (2022) that low-altitude transport of air masses from northern Eurasia explained the measured increase in aerosols

at the location of the Polarstern. The secondary aerosol layer higher up, around 600 hPa, is more likely connected to transport from eastern and southern Asian sources, which dominate the high-altitude transport to the Arctic in spring (Xu et al., 2017). Similar to the Asian dust case presented in Section 3.2.1, moisture is transported close to the surface, below 800 hPa.

Dada et al. (2022) highlight the importance of this event with respect to aerosol-cloud interactions, and therefore climate, with an observed strong increase of cloud condensation nuclei (CCN) concentrations during the intrusion. This event was observed during the MOSAiC expedition, with a unique set of in situ and remote sensing measurements available. However, Figure 3a shows that at the same time, another major combined AR/AeR event reached Greenland. First, a DU AeR is detected, which can affect the formation and characteristics of mixed-phase clouds given the important role of dust as ice nucleating particle (INP) (Murray et al., 2012). Second, because an AR is also associated with the BC and DU AeR, light-absorbing aerosols were likely deposited to the Greenland ice sheet by wet scavenging. As a result, the albedo of the Greenland ice sheet may have been impacted, thereby contributing to accelerate the melting of the cryosphere, through the snow albedo feedback (Skiles et al., 2018). The precise impact of such AeR events needs to be studied as well, despite the lack of in situ measurements. In summary, this case study shows how the use of AeR detection can form the basis of more systematic studies of such extreme aerosol transport events and their impact on polar climate.

3.2.3 2002 Antarctic Peninsula AR

On 19 Feb 2002, a major AR event was detected in the Antarctic Peninsula (AP) and was connected to the final collapse of the Larsen B ice shelf (Wille et al., 2022). This event is also detected as a DU AeR (Figure 4 presents the synoptic situation during this event). However, the DU AeR (yellow shade) and AR (blue shade) have different spatial coverage (Figure 4c). According to our catalog, an AR is detected in the southern Pacific Ocean, which does not extend further south than the tip of South America. However, when using the AR occurrences proposed by Wille et al. (2022) with their detection algorithm based on integrated water vapor (IWV) values instead of IVT, the AR contour (pink shade) made landfall in good agreement with the area where the highest rainfall rates were observed (Figure 4d), except for the southwestern precipitation area over Ellsworth land. All of the precipitation reaching the AP is within the DU AeR contour. In this case, with an AR-only approach, whether using IVT or IWV, the precipitation in Ellsworth land is not associated to the transport event, but by combining IVT AR with IWV AR and DU AeR the whole precipitation event can be traced back to the extreme long-range transport of air masses.

For this event, the DU aerosol and moisture had different source regions. The DU AeR most likely originated from Australia (Figure 4a), while the moisture that contributed to the AR comes from the central tropical Pacific area (Figure 4b), the region where the strongest ARs affecting the AP are generated, as described in Clem et al. (2022). After traveling above the Pacific Ocean, these two air masses generating the AR and AeR meet in a confluent manner, near 40°S-110°W and converge afterwards. This shows how an AR and AeR corresponding to the same event can connect the impacted region to different source areas and therefore transport processes. This case can also illustrate how ARs and AeRs partly follow the same trajectories (here they overlap at around 35°S), but later diverge (here the AeR goes further poleward than the AR and with a more meridional axis) as AR-associated air parcels lose their moisture content when advecting over colder ocean surfaces and isentropically ascend.

As shown by Figure 4c, the DU AeR is detected over the cloud-free region adjacent to the AR. One possible explanation for this is that the extent of the DU AeR is initially the same as the AR, but the DU aerosols present in the AR are scavenged in-

or below- cloud along the way. This would lower their atmospheric concentration and hence the poleward flux, which would no longer be detected as an AeR. This hypothesis is consistent with the vertical profiles during the event (Figure A2): DU is mostly found in large quantities where no liquid/ice water is found, and over the region of lower precipitation along the transect, but the mixing ratio is very low wherever water, including precipitation, is found. Figure A2 also shows, similar to the previous cases, that the transport of aerosols takes place at higher altitude than moisture transport.

In summary, these case studies show that (i) the AeR detection algorithm reproduces well important aerosol transport events, (ii) aerosols and moisture during combined AR/AeR events are not transported at the same altitudes, and (iii) aerosols and moisture do not necessarily follow the same large-scale pathways nor originate from the same area, even though they impact the same receptor region.

3.3 Characteristics of polar AeRs

In this section we present the climatology (1980–2022) of polar AeRs (i.e. poleward AeRs that reach high latitude areas) and show their similarity and differences compared to ARs, including the impacted areas and seasonality. We also explore the trends in the frequency of occurrence of AeRs and ARs between 1980 and 2022 for the Arctic and Antarctic.

3.3.1 Climatology

We present a high latitude poleward AeR climatology and investigate the regions most affected by AeR events and the seasons of stronger activity, in order to establish a comparison with ARs. In the Arctic, BC AeRs are mostly detected in the northern Atlantic, reaching the Greenland and Iceland regions, and in the northeastern Pacific, reaching Alaska predominantly, and the Bering strait area, with a frequency of up to 5 days per year for the 1980–2022 period (Figure 5). To some extent, DU AeRs are found in the same regions as BC AeRs, except for an eastward displacement in the Atlantic where higher frequencies are obtained, and an additional pathway over Russia that does not appear in BC AeRs. Overall, DU AeRs are also more frequent than BC AeRs. Since sources of SS are more evenly distributed around the globe and closer to the polar regions compared to BC and DU, SS AeRs are much less frequent, with a maximum frequency of 2 days per year. They also present a unique spatial distribution: The maximum of SS AeR detection frequency and dominant pathway is located in Russia, far from significant SS sources, where baseline concentrations are very low but fast transport can occur. Although these SS AeRs do not seem to reach the high Arctic, this is an interesting feature showing how different aerosols can trace different pathways. Elsewhere, the detection frequency of SS AeRs is more homogeneous and generally less than 1 day per year. Compared to ARs, BC and DU AeRs have similar frequencies of occurrence and spatial distributions overall, except at higher latitudes, where AeRs can be two times more frequent than ARs, for instance in northern Greenland and the central Arctic.

In the Antarctic, BC AeRs are more frequent than DU AeRs, in contrast to the Arctic. AeRs generally affect similar areas as ARs, except for Queen Maud Land (20 °W–45 °E), which is frequently reached by ARs, but seldom affected by AeRs. The finding for the Arctic that AeRs are more frequent than ARs at higher latitude does not apply for the Antarctic. SS AeRs are less frequent than BC and DU AeRs in the Antarctic too, and predominantly reach the Weddell Sea and Coats Land region (36 °W–20 °W). An important difference between AeRs in the Arctic and the Antarctic is that, in the Antarctic, AeRs (and ARs likewise) tend to be able to reach higher latitudes more frequently. While the frequency of AR/AeR crossing 80 °N is less than 2.5 days per year in the Arctic, they can penetrate as far as 85 °S in West Antarctica with twice the frequency. This suggests a possibly larger impact (clouds, precipitation, albedo) of ARs/AeRs on the Antarc-

tic ice sheet than on the central Arctic sea ice, because of the stronger polar vortex around Antarctica which generally limits intrusions of lower-latitude air masses.

In the Arctic, averaged at the regional scale (65 °–85 °N), the seasonality of AeRs (analyzed using the number of AeR points per month) is similar to that of ARs, with maximum frequency in winter months and minimum activity in summer months, and a correlation of at least 0.69 among these four types of AR/AeR (Figure 6). For ARs, this can be related to higher background levels of moisture in the summertime atmosphere (Rinke et al., 2019), along with the position of the Arctic dome that does not favor long-range transport in summer, including of aerosols (Boyer et al., 2023). This makes the long-range transport relatively less important, as opposed to winter/spring when the polar dome is more expanded which facilitates long-range transport from lower latitudes (Pernov et al., 2022; Boyer et al., 2023). The DU AeR seasonality shown here is consistent with the seasonality of DU transport to the Arctic shown in Böö et al. (2023). SS AeRs stand out, with a stronger seasonality and more rapid transitions between the winter and summer frequencies, resembling more a binary regime shift than a smooth seasonal evolution (cross markers in Figure 6). This latter cycle is harder to interpret as there are few SS AeR events per year (Figure 5), but it may be related to the seasonal cycle of sea ice cover: when sea ice is at its minimum extent, between late spring until late fall, more open ocean is present compared to winter, and therefore more SS is emitted locally. As a result of these local emissions, the background SS loads are higher than in winter, and the relative contribution of transport is thus less important, which is why SS AeRs are less often detected.

In the Antarctic (65 °–85 °S), the seasonality is less clear, especially for BC AeRs which do not feature a seasonal cycle and are, as a result, not correlated with the other three types of AR/AeR. This absence of correlation is interesting as it can signal a more steady occurrence of BC AeRs throughout the year, which provides a more systematic and non-seasonally dependent way of analysing extreme transport events. Here again, the seasonality of SS AeRs is stronger than for the other species, also most likely related to sea ice cover seasonality like in the Arctic. Given how the sulfate content of SS in ice and firn, which varies with seasons, may be used to recover the seasonality of precipitation and reconstruct annual surface mass balance (Goursaud et al., 2019), coupling this feature with SS AeR detection can provide insight for the reconstruction of seasonal climate variations.

3.3.2 Trends

This section investigates the spatial and temporal trends of AeRs, including a comparison with AR trends, in order to assess whether they similarly reflect changes in the climate. Figures 7 and 8 show that ARs feature significantly (at the 95% level) increasing trends at the regional level since the 1980s, despite spatial heterogeneity, with similar magnitudes at both poles. The underlying causes for these trends remain an open question (Wille et al., 2019, 2022). Increasing amount of water vapor in the atmosphere at the mid-latitudes as the climate warms could partly explain this (Gershunov et al., 2017). For the Arctic, changes in circulation, with increasing frequency of blockings also drive the increase in moisture transport (Nygård et al., 2020; You et al., 2022), whereas in Antarctica, trends on the Amundsen Sea Low might explain AR trends in the Amundsen-Bellinghausen Sea (Turner et al., 2013; Wille et al., 2021). Trends in AR activity across Antarctica are similar with previously observed trends, but are slightly sensitive to the choice of the reanalysis product used for AR detection (Wille et al., 2021). Figure 8 illustrates that, overall at the hemispheric level, the evolution of high latitude poleward ARs is closely correlated with the evolution of hemispheric averages of water vapor mixing ratio at 1000 hPa. AeRs on the other hand display a variety of trends depending on the pole and species considered (Figure 7).

BC AeRs tend to generally increase over time in the Arctic, except over the Finland/Russia corridor where a significant decreasing trend is observed (Figure 7). The strongest increase in BC AeRs is found in the North Atlantic, while emissions are steady in MERRA2 in North America over the period. This suggests that the evolution of Arctic AeRs may be driven more by changes in circulation than changes in source intensity. In the Antarctic, BC AeRs are more homogeneously increasing, with only a portion of East Antarctica not showing a significant trend. In parallel, BC emissions decrease in the Amazon region in MERRA2 (Figure A3), which drives the hemisphere-averaged decrease, but strong increases in emissions are found in southern Africa and south Asia. The resulting increasing trend in BC AeRs suggests that either (i) African and Asian BC sources are more important than South American sources for Antarctic-reaching BC AeRs, or (ii) changes in circulation dominate the evolution. Note that averaging emissions only below 30 ° S/above 30 ° N instead of the whole hemisphere, results in the same conclusions (Figure A4).

DU AeRs do not feature significant trends in the Arctic on average, due to slight increases in Northeast America and Siberia compensated by slight decreases over Europe and Alaska (Figure 7). At the same time, emissions are relatively steady in the northern hemisphere (Figure 8). For the Antarctic, a strong increasing trend is observed everywhere (Figure 7), despite a slight decrease in emissions (Figure 8). However, the decrease in emissions hides an important heterogeneity: while DU emissions decrease in Australia over the period, they increase in Patagonia at the same time (Figure A3). The fact that the resulting DU AeR trend has on average a strong increase suggests that the South American DU sources are generally more important than Australian sources for Antarctic DU AeRs.

SS emissions have been increasing globally over the course of the 20^{th} century (Figure A3), driven by increases in wind speed and decline of sea-ice cover (Lapere et al., 2023). However, the corresponding trend in SS AeRs is generally non-significant and even slightly decreasing at higher latitude (over Greenland and Antarctica in particular). This might suggest that the dynamical mechanisms generating SS AeRs have been generally weakening over the last 40 years.

In summary, current trends in AeR (ii) are different from trends in AR, (ii) are diverse depending on the type of AeR (BC, DU, SS), (iii) have clear differences between the poles, and (iv) are not clearly correlated with emission trends. All of the above suggests that AR and AeR detections have the potential to be complementary tools that can be used together for a number of applications, as will be further discussed in Section 4.

3.4 Co-occurrence of strongest AeRs and ARs

This section investigates the strongest AR/AeR of each type that reached Greenland and the AP, between 1980 and 2022. These two regions are often studied in the AR literature, hence their choice as receptor regions here. The top AR and AeR days are ranked based on the cumulated vIxT within an AR/AeR event detected inside the black contours in the left panels in Figures 9 and 10. The top 20 of these events are then analyzed as a composite, and their co-occurrence with other types of AR/AeR is quantified.

For Greenland, the 20 strongest ARs are frequently associated with BC AeRs (70% of events), around 60% of the time with DU AeRs, and less than 20% with SS AeRs (Figure 9a). These top AR events originate from the northwest Atlantic Ocean (Figure A5). In contrast, the strongest BC AeRs affect primarily eastern Greenland, coming from the northeastern Atlantic Ocean or continental North America (Figure A5), and occur mostly independently from the other types of AR/AeR, with co-occurrences in less than 30% of the cases (Figure 9b). Major DU AeRs originate either from the continental North

America or from Northern Africa, where important dust sources exist, and are associated with BC AeRs for up to 75% of cases (Figure 9c). ARs are present for 45% of the top DU AeRs, and SS AeRs are mostly absent. Finally, major SS AeRs are often associated with ARs and BC AeRs (more than 50%), and with DU AeRs only in 40% of cases (Figure 9d). Generally, major ARs tend to be associated with AeRs, but the opposite is not the case. AeRs can occur within relatively dry air masses not classified as ARs.

In the AP, the co-occurrence of all types of AR/AeR is generally more frequent than in Greenland (Figure 10 and A6). Top SS AeRs feature less frequent co-occurrences than the other types of AR/AeR (Figure 10d). 75% of the top ARs are also BC AeRs (Figure 10a), and more than 75% (50%, respectively) of the top DU (BC, respectively) AeRs are associated with co-located ARs (Figure 10b,c). Another difference between Greenland and the AP is that the top AR/AeR for Greenland feature a variety of orientations and thereby source region, whereas in the AP all these events have a similar axis, with an origin near the tip of South America (Figure A6). Trajectories also appear to be more narrow for the AP than Greenland. This can be related to more distributed aerosol sources and more diverse transport pathways in the Arctic. Figure 10 also shows that the top ARs/AeRs reaching the AP are more often coinciding with other types of ARs/AeRs also reaching the AP than it is the case for Greenland (except for SS AeR). Although a more thorough investigation is required to explain this difference, this may suggest that in the AP, extreme AR/AeR events are driven more by the dynamics, since all the quantities are transported, whereas in Greenland those large events may be driven both by transport patterns and emission sources, due to the closer proximity of those sources.

4 Potential applications of polar AeRs

The general characteristics of AeRs and the case studies presented above suggest that AeRs can have relevance for several applications, interesting for both the aerosol and the climate communities. In the following we explore some of these potential applications.

4.1 On the co-occurrence of AeRs and ARs

The association between ARs and AeRs is a crucial feature for cloud properties and for aerosol deposition. BC and DU aerosols are important species when it comes to liquid and mixed-phase clouds, as BC can act as CCN and DU can act as INP. Therefore, when ARs and AeRs are combined, cloud properties can be different compared to AR-only cases, with impacts on cloud albedo and/or precipitation timing. Also, since ARs are important contributors to precipitation in the AP (Wille et al., 2021; Maclennan et al., 2023), ARs that are also AeRs can scavenge (wet removal in and below clouds) the high aerosol content, resulting in deposition to the ice sheet upon precipitation, which can darken snow and ice surfaces, and trigger the ice albedo feedback (Bond et al., 2013; Skiles et al., 2018). The co-localized presence of large amounts of moisture and aerosols can also significantly increase aerosol optical depth through the uptake of water by hygroscopic aerosols, with direct impacts on surface radiation.

These possible impacts are illustrated by the difference in total column and atmospheric surface mass concentration of aerosols, as well as aerosol optical thickness (AOT), during the top 20 combined AR/AeR events (i.e. simultaneous detection of AR, BC AeR, DU AeR and SS AeR) compared to the top 20 AR events without associated AeR in Greenland (Figure A7) and the AP (Figure A8). These top 20 AR/AeR are ranked based on the daily mean vIVT averaged over the region defined by the black contours in Figure A7 and Figure A8.

Over Greenland, atmospheric surface mass concentration of BC and DU increase by up to $15\,\mathrm{ng\,m^{-3}}$ and $1\,\mu\mathrm{g\,m^{-3}}$, respectively, when AR and AeRs occur simultaneously

compared to AR-only cases (Figure A7a), indicating that transport does not only occur at high altitudes in the atmosphere. SS surface concentrations mostly increase over the ocean but the anomaly can reach up to $3\,\mu g\,m^{-3}$ over Greenland. For all aerosols, the total column mass density also has a positive anomaly during AR+AeR events (Figure A7b). Similarly, AOT increases by up to 0.08 in the Greenland region (Figure A7c). The largest increases in AOT are correlated with the largest increases in SS mass. Given the highly hygroscopic nature of SS, the combined presence of high moisture levels through the AR, and SS through the SS AeR, explains this large increase in AOT, which can have major impacts on the radiative balance through the aerosol-radiation interaction. For the AP, similar conclusions can be drawn as for Greenland, except for DU for which the surface transport contributes more to the total column compared to Greenland (similar change in total column, but surface concentrations 10 times larger). Based on Figures A7 and A8, it is important to distinguish between clean and polluted ARs for understanding precipitation, albedo, radiation and melting impact of ARs. AeR detection provides a way to do so, and facilitates conducting more holistic impact studies.

The synoptic conditions are different when AR and AeR occur simultaneously compared to cases when each type of AR/AeR occurs independently, as shown in Figure 11. For Greenland, there is a larger diversity of synoptic situations for the top 20 AR/AeR compared to the AP. The geopotential height anomalies are similar for combined AR/AeR (Figure 11e) and AR-only (Figure 11f) cases, with a strong high centered on Iceland, and a comparatively weaker low above eastern Canada. The cases where only BC AeRs are detected are associated with similar spatial patterns but the low is comparatively stronger, and the high comparatively weaker, in addition to a slight eastward displacement which connects Greenland with North American air masses (Figure 11g). For DU AeR days, the transport is driven by a strong high located over the Norway sea, enabling transport from North Africa but without an associated low pressure system (Figure 11h). In other words, the transport in this case is probably slower, but more sustained and with less wet scavenging. SS AeR cases exhibit, for Greenland as well, circulation patterns different from all the others: a large area of low pressure covering Canada and extending until Europe, and a weaker high near Svalbard (Figure 11i). This synoptic situation leading to local storms can export large amounts of open-ocean-sourced sea spray. As a result, SS AeR may not be as fit as BC and DU AeR for the purpose of characterizing long-range transport from the mid-latitudes.

In the AP, when all types of AR/AeR occur simultaneously, a strong high-low dipole with a longitudinal axis appears (Figure 11a), indicating that air masses originate primarily from continental South America. The situation is similar when ARs with no AeR occur, with the exception of the dipole axis which is tilted and therefore suggests air masses come from the southeastern Pacific Ocean rather than continental areas (Figure 11b). When only BC AeRs are detected, the dipole is weaker, with a reduced intensity of the low in particular, and shifted eastward (Figure 11c), but the typical wave train of high-lows coming from Australia appears more clearly than in the other cases. The composite during DU AeRs (Figure 11d) is similar to BC AeRs, except for the tilt of the dipole which shows the influence of Patagonian dust sources in this configuration. In the case of SS AeRs only, the synoptic situation is different from all the others: a very strong low covers the whole AP, surrounded by a strong high in the southwestern Atlantic Ocean and another high at the Pacific and Southern Ocean demarcation. This situation translates the fact that SS sources are closer to Antarctica (sea spray from the Southern Ocean), compared to the other aerosols, and are thus transported by strong winds associated with local storms during extreme events.

The differences in synoptic circulation described above can partially be attributed to the season during which these top events occur. For Greenland, compound events are mostly found in SON–DJF, with the exception of SS AeRs which are more frequent in DJF–MAM (Figure A9). This last feature can be connected to the sea ice cover at that

season, which implies a more important contribution from long-range transport to Arctic concentrations of SS. Cases with only DU AeR and only SS AeR are similarly found predominantly in JJA–SON in the Antarctic. For both poles, the events transporting all quantities simultaneously (AR+BC+DU+SS) have the same seasonal distribution: 50% occur during wintertime, and another 30% during the fall. This finding suggests that winter-fall weather regimes are more favorable for the occurrence of more intense ARs/AeRs reaching Greenland/AP, in addition to being conducive to a higher frequency of AR/AeR occurrence irrespective of their intensity on average at the poles (as indicated by Figure 6). This similarity in the seasonality of combined events can be leveraged for studying, for instance, the comparative evolution, between the two poles, of the seasonality of extreme transport, over longer time scales.

In summary, differences in synoptic circulation appear when considering the 5 different types of AR/AeR (AR, BC AeR, DU AeR, SS AeR, and all combined), leading to different source/receptor areas during the strongest events. Polar BC AeR and DU AeR are also usually polar ARs and vice versa, which can have a combined impact broader than only affecting aerosols or moisture independently. Therefore they deserve to be treated as compound events, not in isolation. Because of their different pathways, AeRs can sometimes connect relatively dry transport events to their impacts (e.g. precipitation) when ARs are not detected. This analysis supports the idea that adopting a clustering analysis using the 5 types of AR/AeR discussed here should be explored in future work.

4.2 Dry extreme poleward transport

AeRs can provide insight for cases of fast poleward transport of relatively dry air masses, that we have demonstrated to be significantly different from AR in terms of the circulation pattern (see Figure 11). In recent literature (Pohl et al., 2021), AR analogues were analyzed, showing important differences with polar AR events. By leveraging the AeR detection built in this work, future research could try to address the question: what if these AR analogues are AeRs? If so, because of the difference in moisture content and radiation/cloud feedback (due to aerosols), the (thermo)dynamics of these two types of events should be different, despite leading to the analogous situations shown in Figure 11. The compared vertical structures of moisture/aerosol extreme transport events, in particular, could help better describe the underlying physical processes. Adopting a new clustering method accounting for ARs, analogues and AeRs instead of the first two only could pave the way towards a better understanding of the factors contributing to AR-like dynamics, and could help to explain the occurrence of non AR-related extreme temperature events (Wille et al., 2022).

4.3 Analyzing future poleward transport occurrences

Analyzing future AR frequency and intensity is complex. As the climate warms, more moisture is available, which constitutes a trend in the source of AR-carried water vapor (Gershunov et al., 2017), as shown in Figure 8. This trend makes it hard to untangle changes in circulation from changes in atmospheric water vapor content when exploring current and future trends in ARs (Rinke et al., 2019; Bintanja et al., 2020). In addition, the AR response to future climate change is highly dependent on the chosen detection tool (O'Brien et al., 2022; Shields et al., 2023). For natural aerosols, the emission sources are not expected to feature strong trends in future scenarios, although more sea salt (Lapere et al., 2023) and possibly slightly more dust (Zhou et al., 2023) can be expected under a changing climate. Local sources of anthropogenic aerosols such as BC are also expected to change moderately, particularly in the Arctic with increased shipping traffic (Corbett et al., 2010). However, the aerosol trends are less directly connected to the warming temperatures compared to the changes in moisture transport (Held & Soden, 2006).

AeRs can offer robust and key information on the dependence of intrusions and ARs on climate change. The implementation of specific simulations, with controlled aerosol emissions, would make it possible to assess the future evolution of atmospheric intrusions considering only variations in atmospheric dynamics. The assessment of the future evolution of the frequency and intensity of ARs could then be treated by eliminating the increase in frequency of occurrence resulting directly from the Clausius-Clapeyron process. Another method could consist of introducing idealized aerosols with different residence times, or other tracers, in a general circulation model (Krinner & Genthon, 2003) and then to analyze the resulting AeRs. Applying this approach based on tracer age for different climates would allow to analyse the climatologies of poleward transport, including in future climate.

4.4 Ice core analysis of past AR activity

The reconstruction of AR variations in past climate has been proposed through the analysis of water isotopes in ice cores, using the δO^{18} ratio (Servettaz et al., 2023), which can be related to changes in local temperature over long time scales (Jouzel et al., 1997). However, the use of the δO^{18}-temperature relationship in ice cores is complex, as it is related to changes in air mass origins, transport, sublimation of hydrometeors, post-depositional effects as well as diffusion in the firn (Werner et al., 2001; Krinner & Werner, 2003; Buizert et al., 2014; Casado et al., 2018; Cauquoin et al., 2019). Moreover, a direct relationship between δO^{18} or d-excess anomalies and temperature is not systematic (Wahl et al., 2022) and is insufficient to retrieve AR occurrence using this proxy alone. Aerosol analysis, through AeRs, could complement water isotopes to retrieve past occurrences of extreme transport events, using a combined δO^{18}-aerosol analysis, since changes in aerosol content in ice cores could result from changes in meteorology (Levine et al., 2014; Rhodes et al., 2018). This connection can also be made for longer time scales, including paleoclimate reconstruction (Wolff et al., 2006).

4.5 Understanding aerosol-climate interactions in polar regions

Aerosols influence both the formation and evolution processes within clouds, acting as CCN or INP. The latter, because of their scarceness and the predominance of ice and mixed-phase clouds in the Arctic and over Antarctica (Matus & L'Ecuyer, 2017), condition the cloud radiative effect and therefore the energy budget of these regions, making them critical for understanding and predicting the polar climate (Murray et al., 2021). The systematic identification of ARs and AeRs could be central in helping elucidate the predominant CCN and INP sources originating from rapid transport to the poles. Aerosol-cloud interactions within ARs have yet to be studied in detail. Depending on the meteorological conditions and the aerosol content and type within ARs, the cloud properties can be affected, as well as the precipitation timing which can be either accelerated or delayed. Conversely, aerosols can be washed away by intense precipitation during an AR, as was shown here for the February 2002 AR event in the AP. Comparing combined AR/AeR events with AR-only events could be an efficient way to quantify these interactions.

In addition to affecting clouds and precipitation, aerosols can darken snow and ice surfaces upon deposition and lower their albedo, triggering the ice albedo feedback (Bond et al., 2013; Skiles et al., 2018). Non-polluted ARs or combined AR+AeR likely have different impacts on the polar ice sheet, which deserves closer investigation, particularly in connection with the observed polar amplification in which ARs and aerosols could play an important role (Wendisch et al., 2023; Zhang et al., 2023).

Finally, the study of transport events of aerosols to the high latitudes usually relies on their detection from satellite or from field campaigns. Satellite measurement of aerosols in polar regions is complex and therefore limited, for several reasons. First, sea

ice is too bright a surface for sensors to accurately separate the contribution to back-scattering from the ground and from aerosols (Mei et al., 2013). Second, cloud cover is predominant throughout the year both in the Arctic and Antarctic (Eastman & Warren, 2010; Lachlan-Cope, 2010), which impedes the retrieval of valid aerosol data. Field campaigns and ground-based measurements are also more limited in these remote regions. As a result, some important aerosol transport pathways or major events can be missed. The systematic detection of AeRs using reanalysis or models can help identify all important events more exhaustively, which is particularly important given the current attention for a better quantification of aerosol-cloud interactions in polar regions. For this, dedicated high-resolution climate modeling of the detected events can help to provide a better understanding.

4.6 Adapting AR algorithms for heat transport

The AeR detection developed here shows that the concept of AR detection can be extended to transported quantities other than water vapor. Another quantity of interest could be heat (Komatsu et al., 2018). The increased meridional latent heat transport (LHT) through ARs was shown for the mid-latitudes, in connection with the moisture transport, but the effect on sensible heat transport (SHT) is less clear (Shields et al., 2019). However, Shields et al. (2019) also show that under climate change scenarios, the increase in the 300 hPa meridional wind speed is a stronger driver of the increase in AR-related SHT than the 850 hPa meridional wind speed. This transport in the upper troposphere is also characteristic of the aerosol transport in AeRs as shown in the different case studies in this work. The aerosol transport occurring higher up also connects to the findings from Papritz et al. (2022), who found that air subsiding from the mid-troposphere into the boundary layer is as important an airstream as surface fluxes for the transport of moisture to the Arctic in wintertime. Using similar algorithms for heat transport as developed for ARs and AeRs, and cross comparing ARs, AeRs and heat transport events could allow the community to understand how moisture, aerosols, clouds, latent heat release and heat advection interact during these events, and quantify how these interactions impact the heat budget at high latitudes.

4.7 Limitations

Future work building on the possibilities offered by polar AeR detection should however be careful to keep in mind that AeRs have limitations, both from the point of view of their capability and their interpretation.

4.7.1 Aerosol sources

Because aerosol sources over the globe are generally more localized than moisture, when analysing specific regions of the Arctic or Antarctic, there is a risk of over-sampling certain trajectories that connect source and receptor regions. For example, when studying the AP, trajectories associated with Patagonian dust events could be over-represented due to the short distance and high activity of this source. This is particularly true for the Arctic where aerosol sources of all types are generally closer than in the Antarctic, which leads to transport events occurring more frequently. As a result, extreme transport events described by AeRs have a comparatively smaller importance when it comes to the annual aerosol budget in the Arctic than in Antarctica.

However, this possible sampling bias does not seem to appear in the climatologies presented in this work as both ARs and AeRs feature similarities in spatial distribution and frequencies, despite different source regions (moisture mostly comes from the ocean, whereas BC and DU are mostly emitted from land). In this respect, one could argue that, perhaps, AeRs are a signal of extreme transport of the global background aerosol, rather than a source-receptor connection. In that case, for example, a DU AeR in the Antarc-

tic would not necessarily describe the transport of Patagonian or Australian DU, but extreme transport of air masses not coming from DU source regions, which carry background DU levels throughout the troposphere. This does not appear to be what happens in the case studies presented in Sections 3.2.1 and 3.2.2 where concentrations are much higher than background, but this could partly explain the lack of correlation, on average, between emission trends and trends in AeR that we show in this work.

4.7.2 Sea salt aerosol

Among the different aerosol types considered here, SS AeRs seem to be a less adapted tool when it comes to the potential applications of AeRs. First, because sources are more widespread and closer to the poles, particularly in the Southern Ocean, SS AeRs are quite rare and seem to relate more to local large storms, rather than extreme transport of mid-latitude air masses. Furthermore, simulations show that the interpretation of sodium variability in Arctic ice cores can be either related to sea ice changes or meteorological factors, and depends on the area where the ice cores are drilled (Rhodes et al., 2018). As a result, the connection between sodium in ice cores and circulation patterns can be difficult to interpret, although at shorter time scales and for Antarctica, ice core sodium can be more directly related to meteorology (Levine et al., 2014). In comparison, BC and DU in ice cores might be more straightforward to relate to atmospheric processes as the sources are further away, and to some extent less seasonally dependent as they are not connected to sea ice cover variations.

Furthermore, SS can undergo re-suspension in sea ice and snow regions through the process of blowing snow (Yang et al., 2008; Frey et al., 2020). SS aerosols that were deposited onto coastal regions can thereby be transported further inland and eventually end up in non-coastal ice cores. As a result, SS aerosols that may have been brought to the poles through SS AeRs can be transported several days later and several hundred kilometers away from the AeR region. This can create a bias in the connection between ice core sodium and AeRs.

4.7.3 Current state of aerosol modeling

The representation of the polar aerosol budget in models and reanalyses is still uncertain. Emissions, transport and deposition are diversely represented. In particular, DU and SS mass concentrations are usually overestimated at high latitudes, including in MERRA2, and differ depending on the model/reanalysis considered (Böö et al., 2023; Lapere et al., 2023). Because we only evaluate extreme events here, defined based on a relative threshold, this should not be a problem for AeR detection, but for impact studies this may be a limitation.

Furthermore, aerosol-radiation and aerosol-cloud interactions are still challenging to represent in climate models and reanalyses. In particular, the effect of aerosol content in ARs and the role of AeRs in triggering precipitation, designated above as a topic that can benefit from AeR detection, is not straightforward to estimate. The extent to which AeRs exert a meteorological feedback, which could help self-sustain or dampen the transport, is also not possible to evaluate at this state of climate modeling, although this would be critical information for understanding the physical processes controlling extreme transport events. Similarly, even in the latest generation of models, transport and deposition (dry and wet) processes in polar regions are challenging to accurately model, which can affect both the quality of the AeR detection and the impact studies.

However, these aerosol-climate interactions are better represented in smaller scale models, such as regional chemistry-transport models (CTMs) and regional climate models (RCMs). We believe that using the AR/AeR catalogs can help identify test cases of interest which can then be simulated using high-resolution CTMs/RCMs. Evaluation and

sensitivity analysis for these cases can help isolate and quantify the impact on clouds and precipitation, and eventually on cryosphere melting, of the aerosols present in AeRs. Furthermore, deposition fluxes of BC and DU can be computed, and the impact on snow and ice albedo can be evaluated.

5 Conclusions and perspectives

In this work, we create a polar-specific AeR catalog for BC, DU and SS aerosols, by leveraging and adapting an AR detection algorithm. We validate the AeR detection by analysing case studies and comparing with AR climatologies, including evaluating the sensitivity of detection to the threshold chosen. We present the climatology and seasonality of polar AeRs, in the Arctic and Antarctic, and show that they are often similar to ARs, but also have different characteristics that have added-value for understanding poleward transport processes. We also present the trends in AeRs over the last 40 years, which do not show a connection with the evolution of aerosol emissions. In comparison, AR trends are well correlated with the increase in atmospheric moisture.

The detailed study of three major AR and AeR events shows that they can originate from different remote source regions and eventually converge in a confluent manner resulting in similar trajectories just before landfall. These case studies also show that aerosols and moisture are not transported at the same altitudes. Overall, they indicate that a more holistic approach of extreme transport events is needed instead of moisture-only or aerosol-only analyses. Composites over the strongest AR/AeR of each type further illustrate the complementary nature between AR and AeR, as they are associated with different synoptic circulations. These composites also show that co-occurring AR and AeR bring large amounts of aerosols near the surface compared to AR events with no AeR.

The potential applications of AeRs that should be explored in future work include, for example:

1. **Gaining a holistic understanding of rapid transport from the mid-latitudes to the poles.** Because the dynamics involved in AeR and AR can be similar in some cases, but the sources, or zones of uptake and uplift of moisture differ from aerosols, combining both ARs and AeRs can provide a more holistic understanding of the transport of mid-latitude air masses to the poles. This can aid in better understanding the underlying physical processes and their feedbacks, that are critically important for polar climate including, for example, cyclogenesis, blocking amplification, clouds, and precipitation.
2. **Understanding aerosols preserved in ice, firn, and snow.** AeR detection is one tool that can be used to help understanding how aerosols arrive on the ice sheets and aid in interpreting chemical signals stored in polar ice, firn, and snow. AeR catalogs take into account changes in emissions, transport and wet or dry deposition, which is important for understanding what species are stored in the ice core record and how the associated air masses were transported from the mid-latitudes to the poles. The approach could also be extended for future climates, and to tracer age analyses based on controlled emissions of various tracers, giving information on transit times and pathways to the ice sheet.
3. **Quantifying the impact of extreme aerosol transport on polar climate.** Systematic studies of major aerosol intrusions through AeR can provide a way of quantifying both the aerosol direct (aerosol-radiation interactions) and indirect (aerosol-cloud interactions) effects, as influenced by transport from the mid-latitudes. Event detection and clustering can, for example, suggest AeR impacts on polar clouds and precipitation.

In summary, we provide a catalog of AeRs that are a new and unique tool that can provide a better understanding of polar climate and its connections with the mid-latitudes.

Open Research

The detection catalogs for AR and AeR, based on MERRA2 vertically integrated fluxes at $1^\circ \times 1^\circ$ spatial resolution and covering the period 1980–2022, along with the processing and detection codes, are available at `https://doi.org/10.5281/zenodo.8082768` (Lapere, 2023).

Author contributions

Conceptualization: RL, JT, VF, HA, LM; Methodology: RL, JT, VF, JA, AE; Visualization: RL; Formal Analysis: RL, JA; Writing - Original Draft: RL, JT, VF, HA; Writing - Review & Editing: JA, AE, LM, JR, AS, JW, PZ;

Acknowledgments

This project has received funding from the European Union's Horizon 2020 research and innovation programme under grant agreement No 101003826 via project CRiceS (Climate Relevant interactions and feedbacks: the key role of sea ice and Snow in the polar and global climate system). VF and JW acknowledge support from the Agence Nationale de la Recherche project ANR-20CE01-0013 (ARCA). AE acknowledges the EU H2020 FORCeS project, contract No 821205. We acknowledge J. Schmale at École Polytechnique Fédérale de Lausanne and her team/collaborators who conducted the aerosol measurements during the international Multidisciplinary drifting Observatory for the Study of the Arctic Climate (MOSAiC). These data sets, already published in Dada et al. (2022), were used in this work for the validation of our methodology. We are grateful for their commitment to open data sharing, which advances scientific knowledge.

Figures

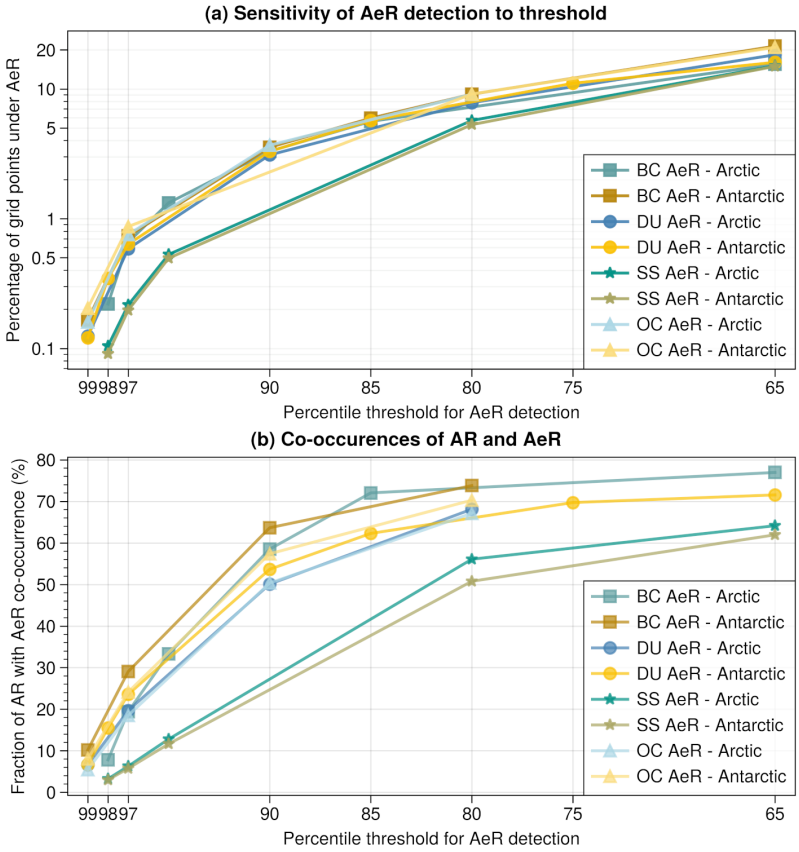

Figure 1. AeR detection - threshold sensitivity. (a) average percentage of AeR grid points as a function of the detection threshold, for BC AeR (squares), DU AeR (circles), SS AeR (stars) and OC AeR (triangles), in the Arctic (60 °–85 °N - blue) and the Antarctic (60 °–85 °N - yellow). (b) Fraction of AR grid points with co-occurring AeR as a function of the AeR detection threshold.

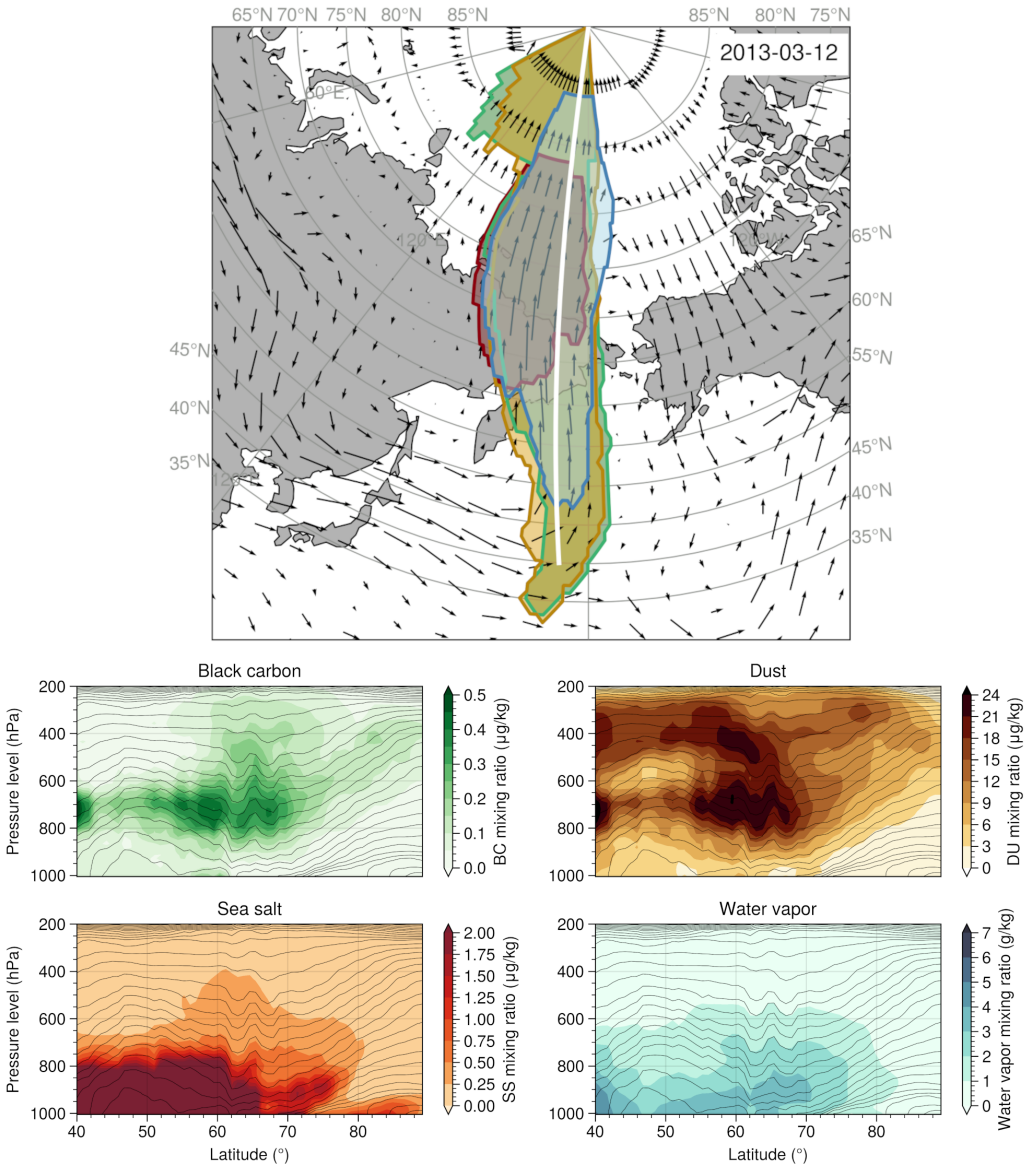

Figure 2. 2013-03-12 Asian dust transport to the high Arctic. Top: detection of AR (lightblue), BC (green), DU (yellow) and SS (red) AeRs, and 500 hPa wind (arrows) on 2013-03-12. Bottom: vertical profiles of BC, DU, SS and water vapor mixing ratio along the white transect in the top panel. Contours indicate constant levels of equivalent potential temperature (isentropes).

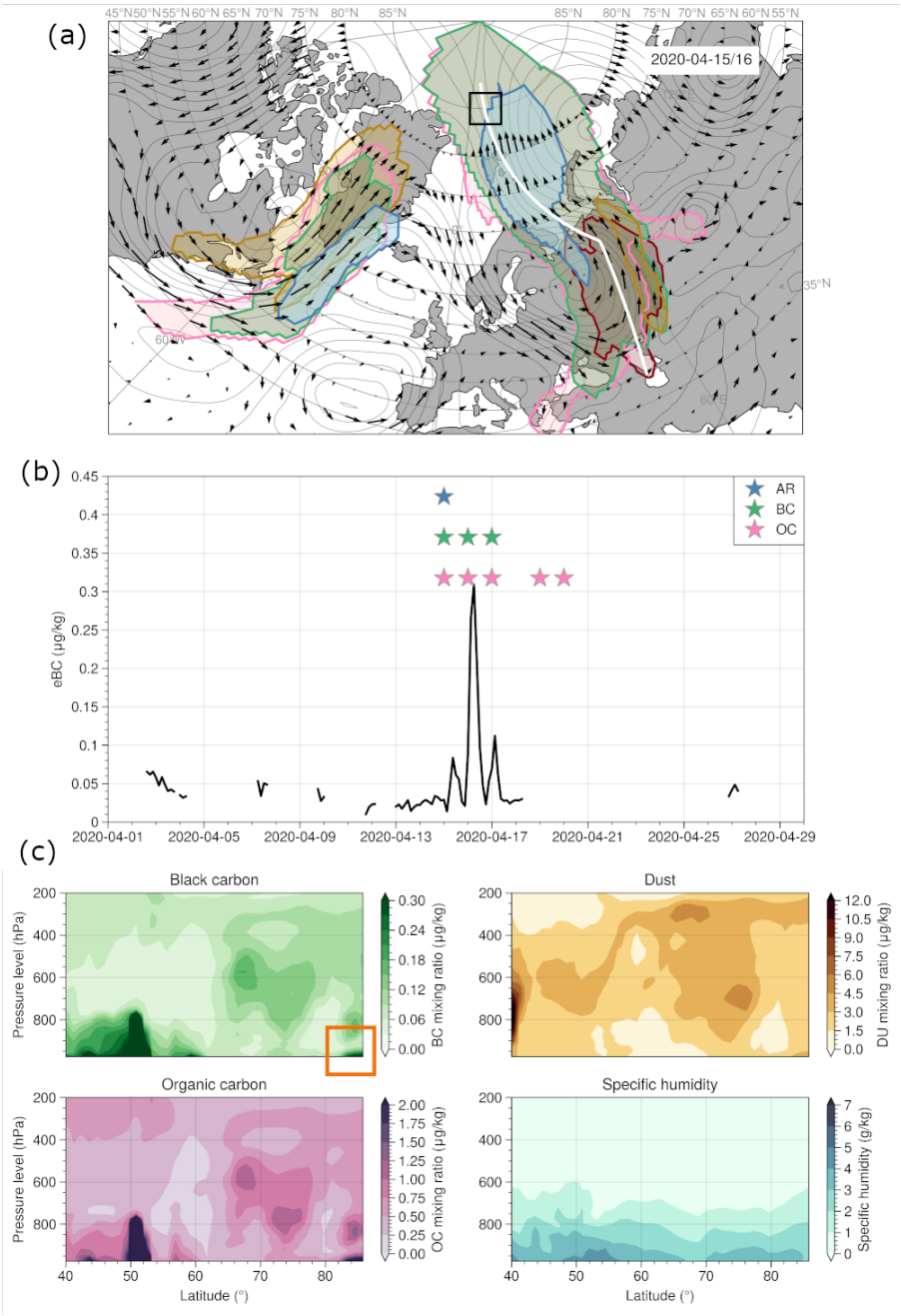

Figure 3. 2020-04-15 pollution transport to the Arctic during MOSAiC. (a) synoptic circulation and AR/AeR detection on April 15-16. Blue shade is AR, green shade is BC AeR, pink shade is OC AeR, yellow shade is DU AeR, red shade is SS AeR. Wind field (arrows) and geopotential height anomalies (contours) are superimposed on the detections. The location of the ship is indicated by the black square. (b) time series of equivalent BC measured onboard the ship (black line - data from Heutte et al. (2022) converted from concentration to mixing ratio assuming air density of $1.2922\,\mathrm{kg\,m^{-3}}$) and corresponding AR/AeR daily detections (stars - blue is AR, green is BC AeR, pink is OC AeR) in the ship area (black square in panel a). (c) Vertical profiles of aerosol and water vapor mixing ratio along the white transect represented in panel a. The orange rectangle indicates the area where the ship was located.

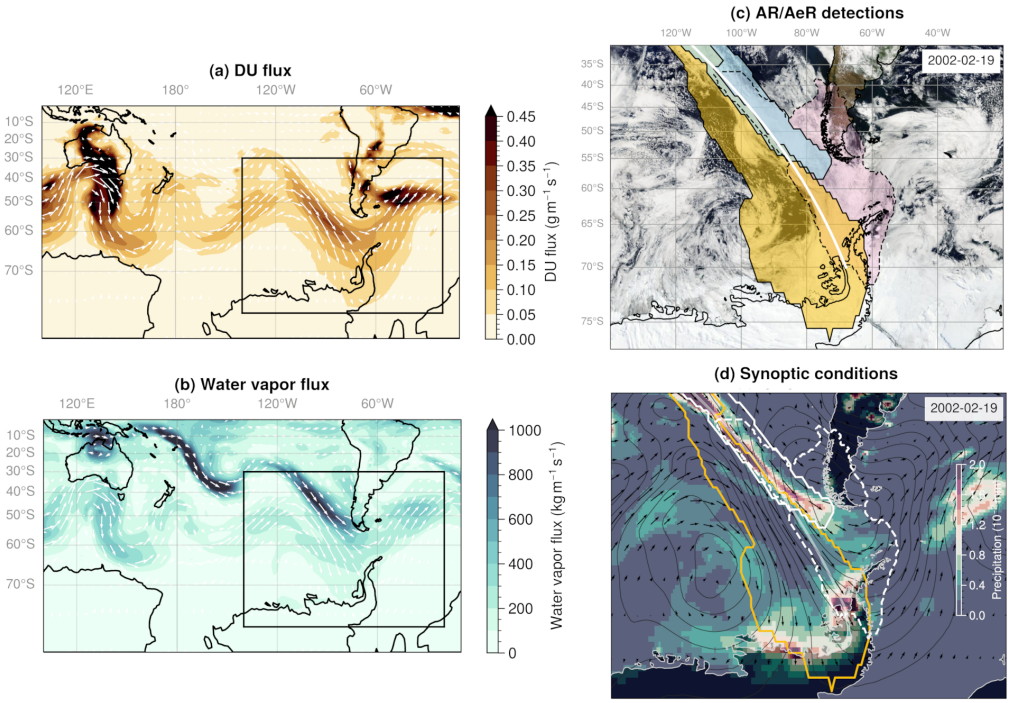

Figure 4. 2002-02-19 Antarctic Peninsula AR. Vertically integrated DU (a) and water vapor (b) flux (zonal and meridional) from MERRA2 on 2002-02-19 (colormap) and associated 500 hPa wind field (arrows). (c) detected AR (blue shade) and DU AeR (yellow shade) near the AP on 2002-02-19. Pink shade with dashed contour is the AR detected using IWV instead of IVT (Wille et al., 2022). Background: Moderate-Resolution Imaging Spectroradiometer (MODIS) Terra corrected reflectance, downloaded from the Earth Observing System Data and Information System (EOSDIS) Worldview (NASA, 2013). (d) detected AR (white contour), DU AeR (yellow contour) and IWV AR (white dashed contour), 500 hPa geopotential height anomaly (black contours), 500 hPa winds (arrows), and precipitation (colormap). The extent of the right-hand panels corresponds to the black box in the left-hand panels.

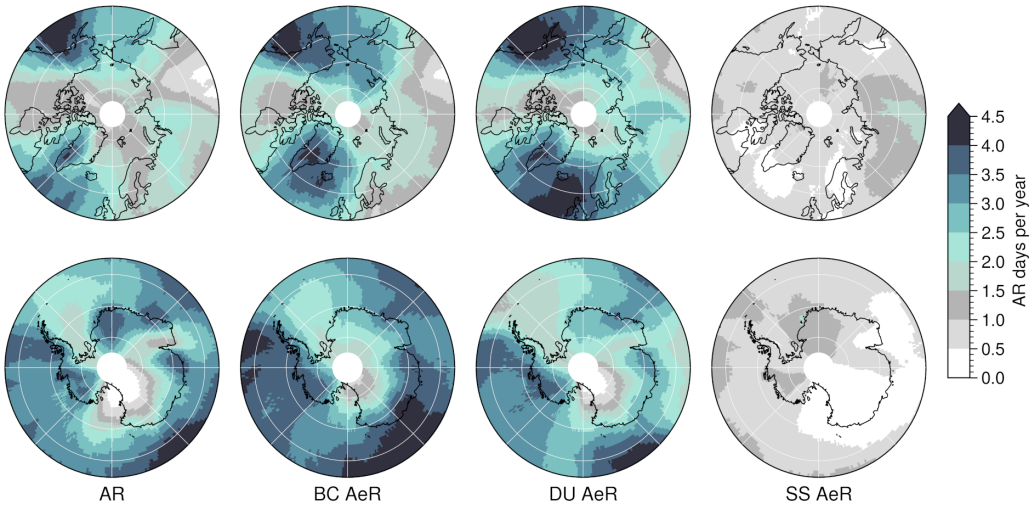

Figure 5. Climatology of polar ARs and AeRs. Frequency of AR (left), BC AeR (middle-left), DU AeR (middle-right) and SS AeR (right) detection, expressed as a number of days per year under AR/AeR for each grid point. This climatology covers the period 1980–2022.

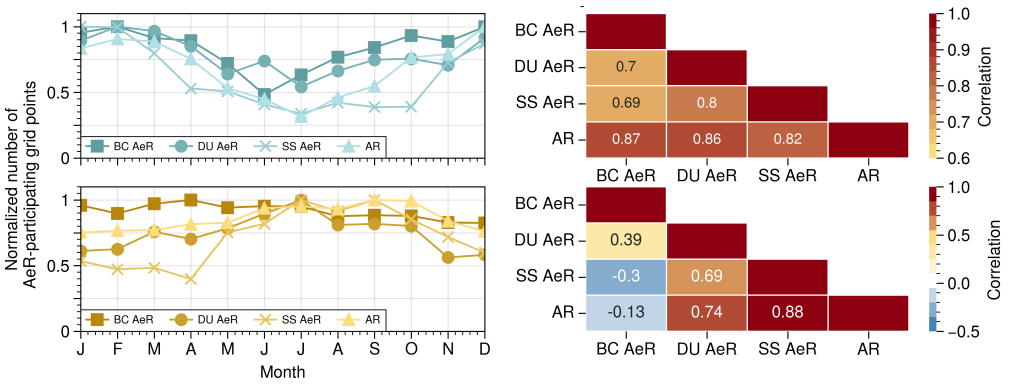

Figure 6. Seasonality of polar ARs and AeRs. Normalized monthly average frequency of AeR and AR grid points (left) for the Arctic (65 °–85 °N - top) and the Antarctic (65 °–85 °S - bottom) and correlation matrix between these seasonal cycles (right). Period 1980–2022.

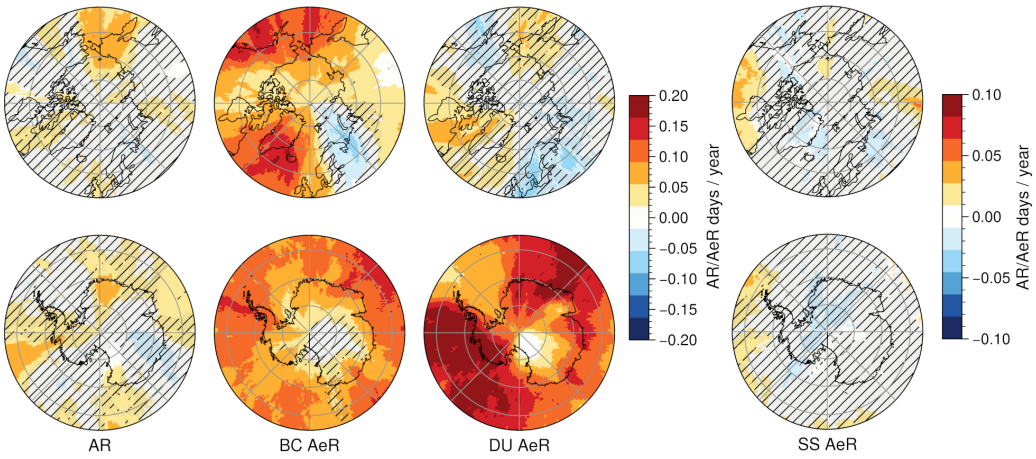

Figure 7. Trends in polar ARs and AeRs. 1980–2022 trends in AR (left), BC AeR (middle-left), DU AeR (middle-right) and SS AeR (right). Trend coefficients are computed as a linear regression of the time series of yearly AR/AeR over the period, for each grid point. Hatching indicates non-significant trends at the 95% level against a Mann-Kendall test.

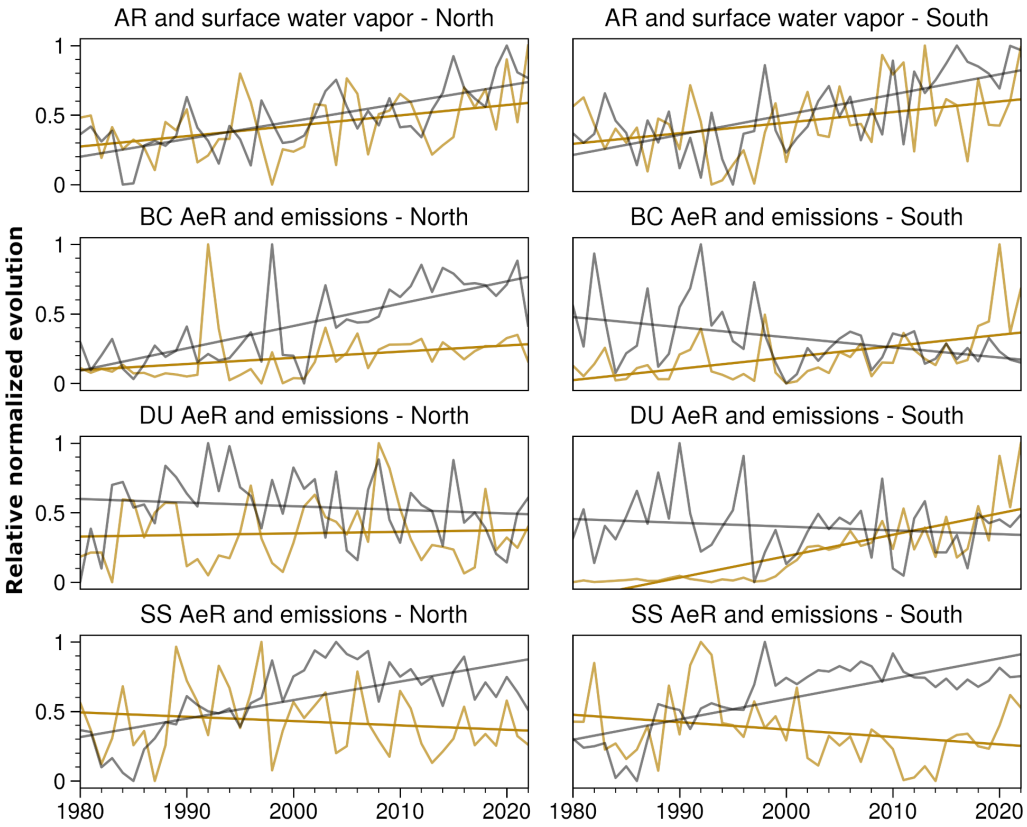

Figure 8. Evolution of polar ARs and AeRs. Time series of the annual number of AR and AeR (yellow line) in the Arctic (65 °–85 °N - left) and Antarctic (65 °–85 °S - right), and evolution of annual emissions of aerosols (1000 hPa water vapor mixing ratio for AR) in the northern (0 °–90 °N) and southern (0 °–90 °S) hemisphere (black line). Straight lines indicate linear regressions. All time series are normalized to vary between 0 and 1 in order to compare the relative trends. Period 1980–2022. NB: emission trends remain similar if the cut-off is performed at 30 ° latitude instead of the equator (see Figure A4).

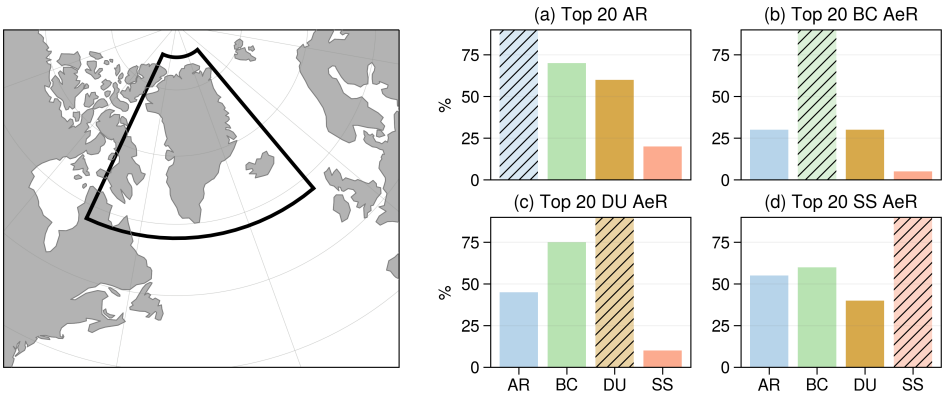

Figure 9. Top 20 ARs and AeRs in Greenland. Blue bars are AR, green bars are BC AeR, yellow bars are DU AeR, red bars are SS AeR. (a) composite of the top 20 ARs in terms of cumulated vIVT reaching Greenland, and associated AeRs. (b) same as (a) but for the top 20 BC AeR. (c) same as (b) but for DU AeR. (d) same as (b) but for SS AeR. The area considered for compositing is the black box in the left panel. The percentage corresponds to the fraction of days for which other AR/AeR types are detected at the same time as the top AR/AeR.

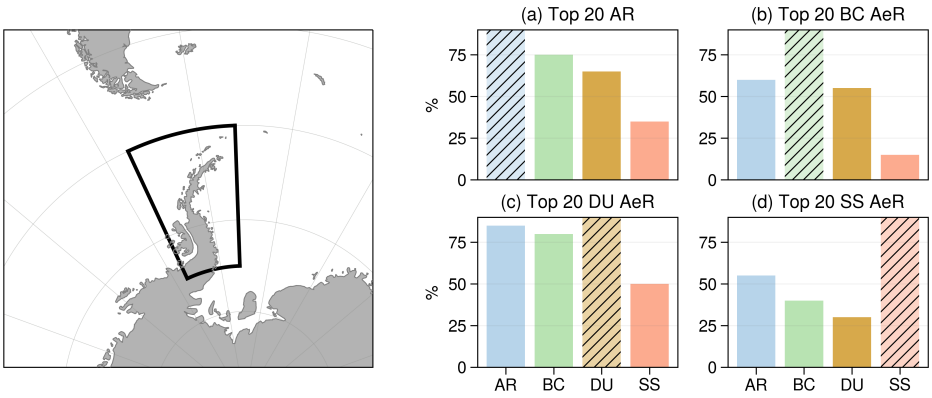

Figure 10. Top 20 ARs and AeRs in the AP. Same as Figure 10 but for AR/AeR reaching the AP.

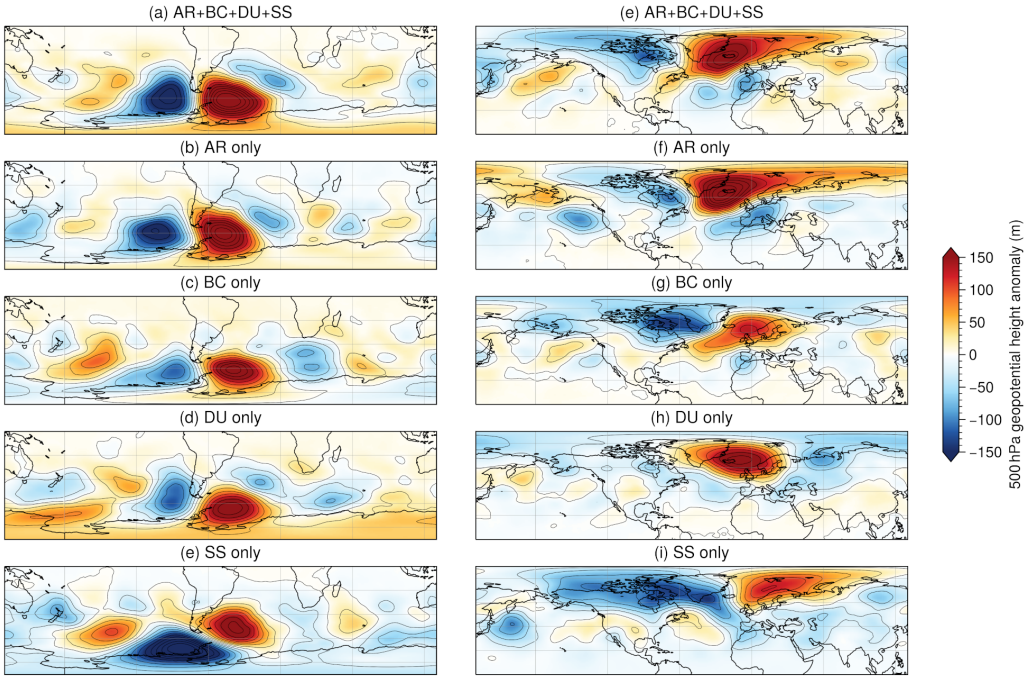

Figure 11. Geopotential height anomalies during top events. Composite of 500 hPa geopotential height anomalies for the top 20 events of 5 different types reaching the AP (left) and Greenland (right). (a, e) co-occuring AR and AeR of all aerosols. (b, f) AR only with no AeR. (c, g) BC AeR only. (d, h) DU AeR only. (e, i) SS AeR only. Geopotential height from MERRA2.

Appendix A

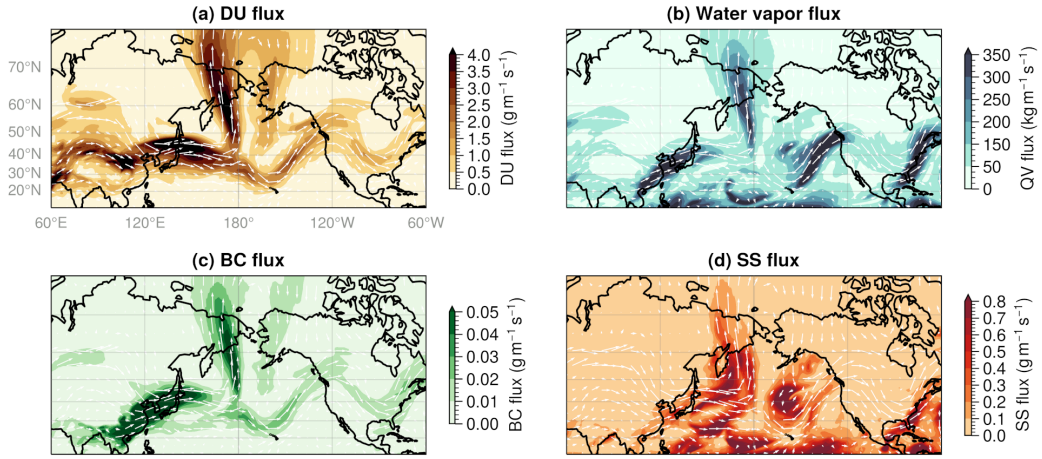

Figure A1. Fluxes on 2013-03-12. Vertically integrated DU (a), water vapor (b), BC (c) and SS (d) flux (zonal and meridional) from MERRA2 on 2013-03-12 (colormap) and associated 500 hPa wind field (arrows).

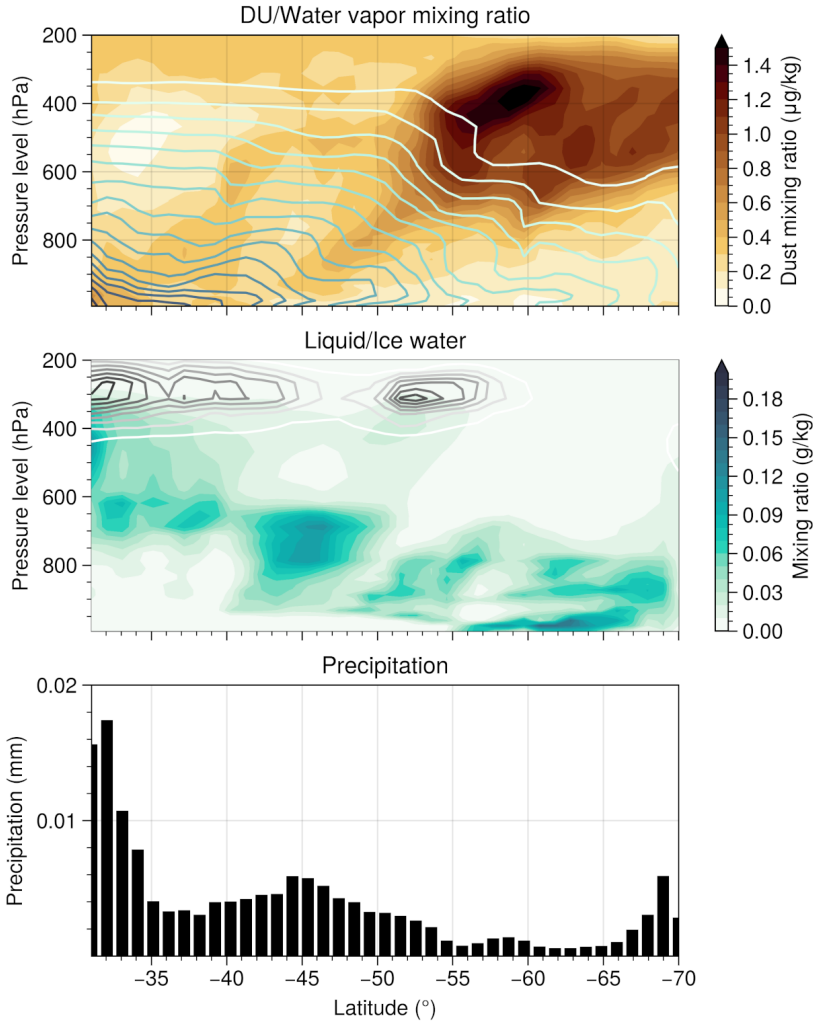

Figure A2. Vertical profiles during the 2002-02-19 AP case. Vertical profiles along the white transect in Figure 4c. Top: DU (colormap) and water vapor (contours) mixing ratio. Middle: Liquid (colormap) and ice (contours) water mixing ratio. Bottom: surface precipitation.

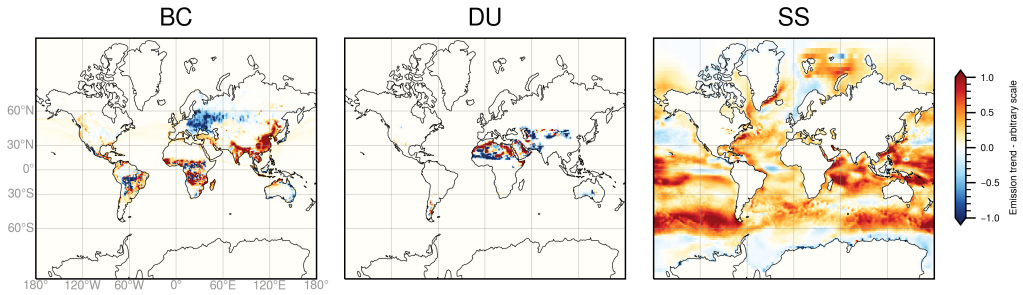

Figure A3. Aerosol emission trends. Trends in yearly aerosol emissions in MERRA2 over the period 1980–2022.

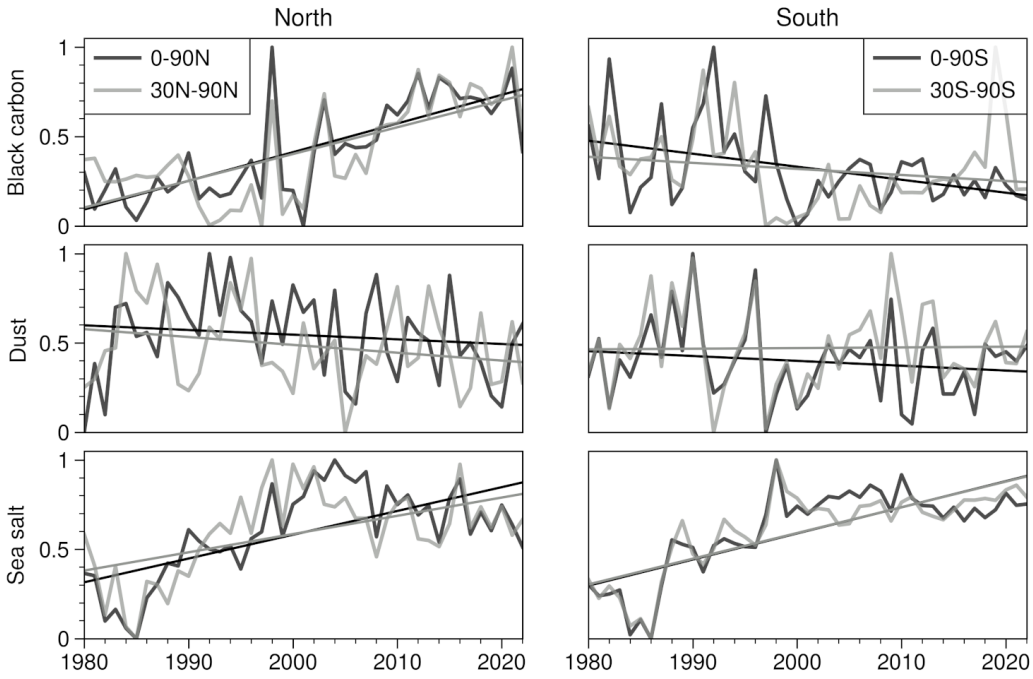

Figure A4. Aerosol emission trends. Sensitivity of emission trends to the cut-off latitude. Black is for a cut-off at the equator, grey is for a cut-off at 30 ° N-S.

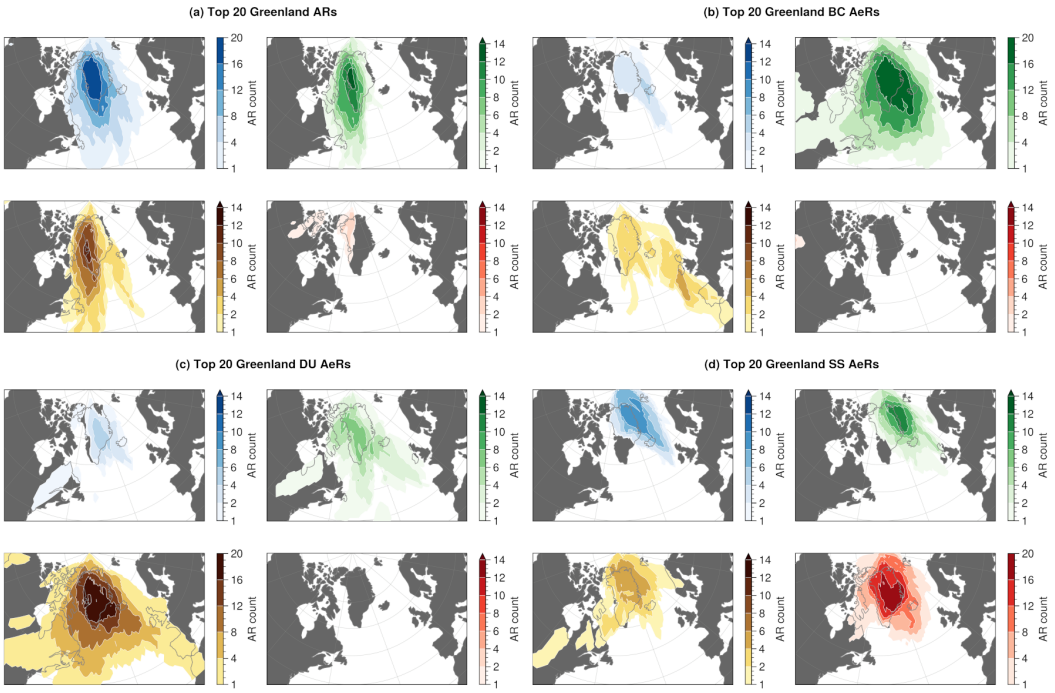

Figure A5. Top 20 ARs and AeRs in Greenland. Blue shades are AR, green shades are BC AeR, yellow shades are DU AeR, red shades are SS AeR. (a) composite of the top 20 ARs in terms of cumulated vIVT reaching Greenland, and associated AeRs. (b) same as (a) but for the top 20 BC AeR. (c) same as (b) but for DU AeR. (d) same as (b) but for SS AeR. AR/AeR counts correspond to the number of AR/AeR days for the top 20 dates, for each grid point.

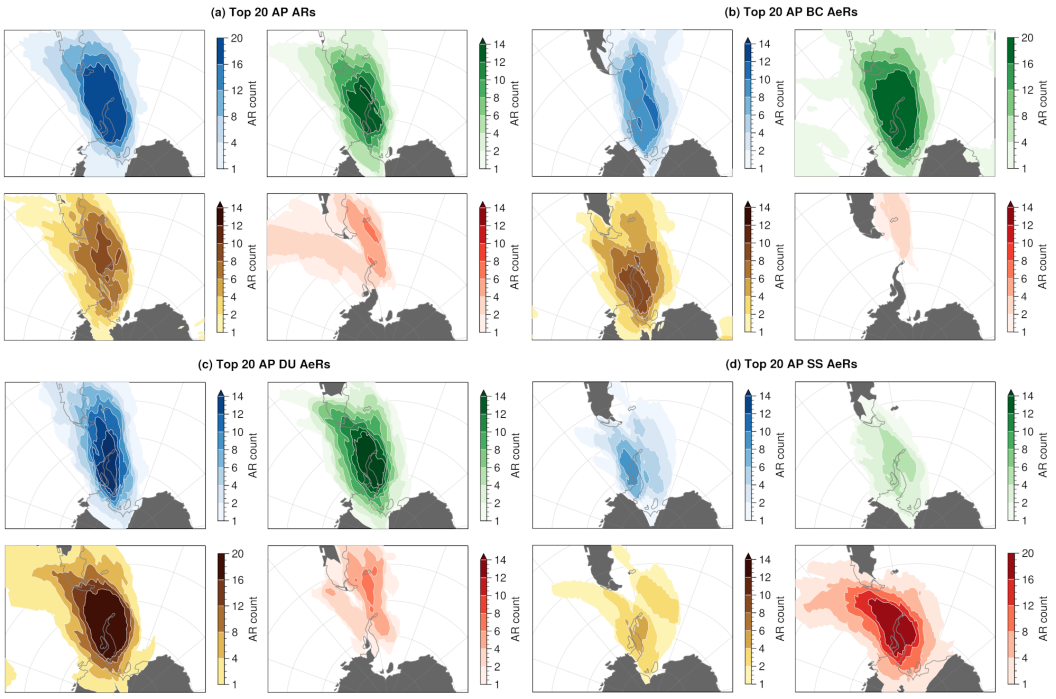

Figure A6. Top 20 ARs and AeRs in the AP. Same as Figure 10 but for AR/AeR reaching the AP.

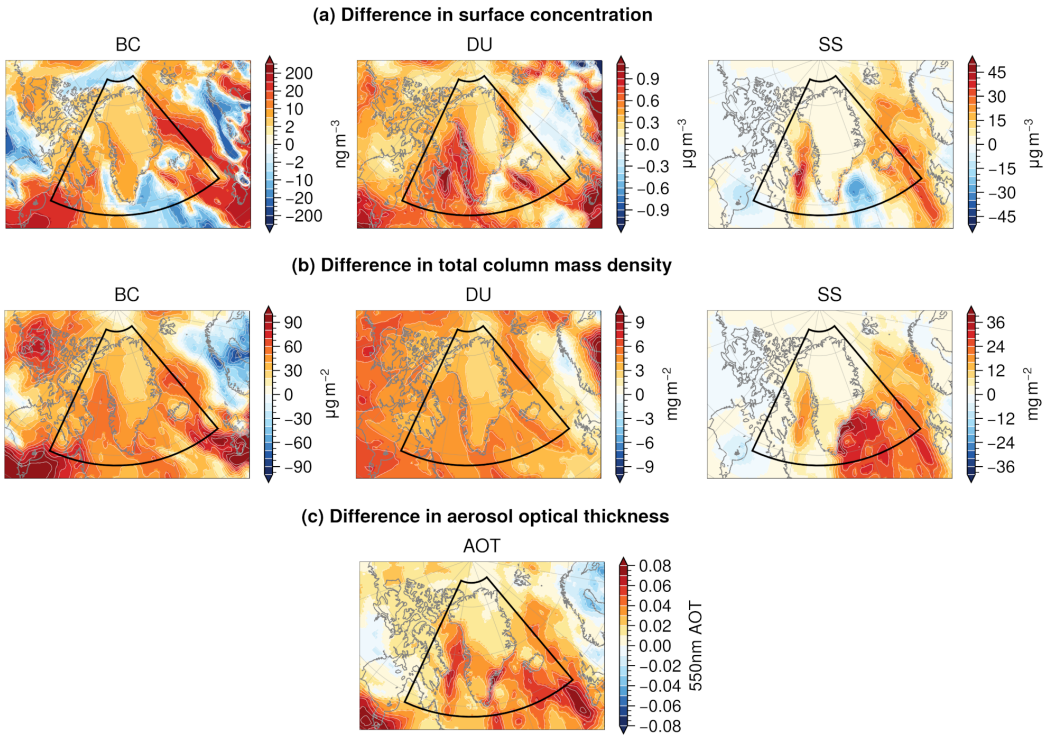

Figure A7. Effect of AeRs on aerosol mass and optical properties. Difference in (a) surface mass concentration of aerosols, (b) total column mass concentration of aerosols, and (c) aerosol optical thickness, between days with combined AR/AeR and days with AR only. The days/area considered for compositing are the same as in Figure 11a and Figure 11b.

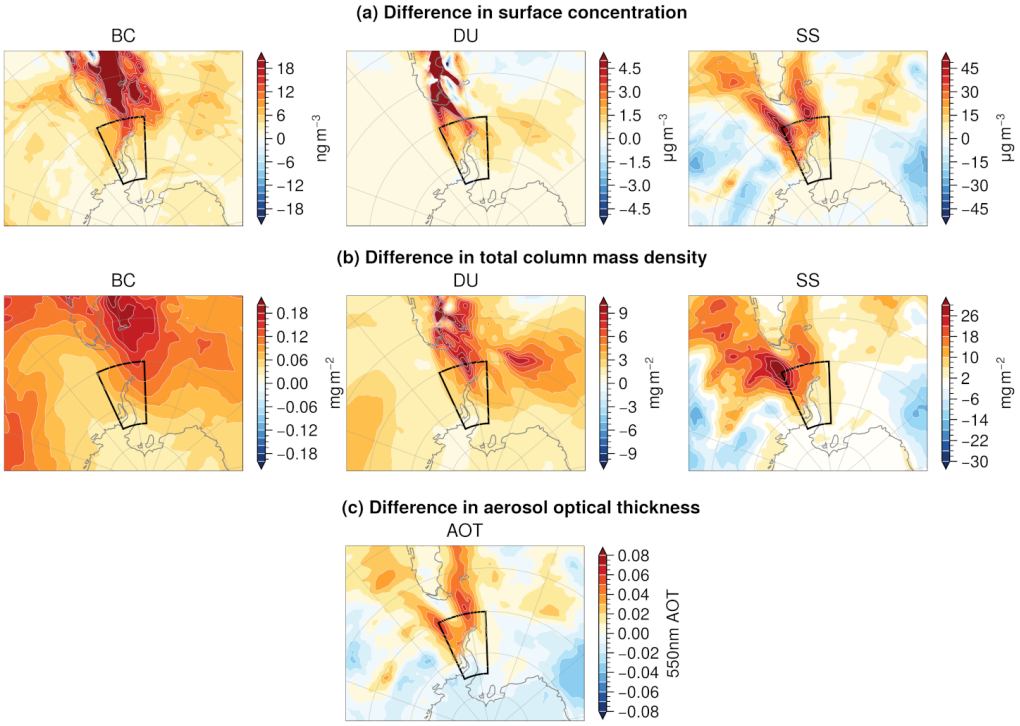

Figure A8. Same as Figure A7 but for AP events.

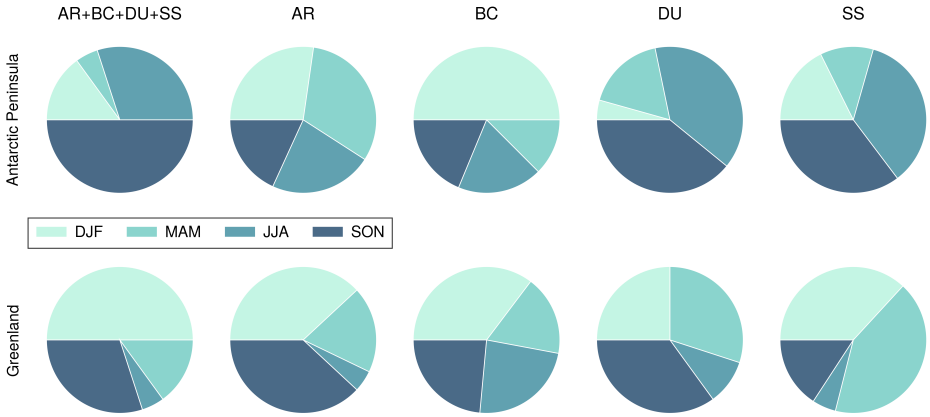

Figure A9. Seasonal distribution of the top 20 AeRs/ARs. Frequency of occurrence, by season, of the top 20 AR/AeR composites from Figure 11.

A1 Adaptations to and validation of AR detection

The method for the detection of ARs and AeRs is based on the algorithm described in Wille et al. (2019, 2021). In this scheme, the criterion variable is the integrated meridional flux of water vapor ($\mathrm{v}IqT_{\mathrm{Wille}}$) between the 900 hPa and 300 hPa pressure levels (Eq. A1), taken every 3 hours.

$$\mathrm{v}IqT_{\mathrm{Wille}} = -\frac{1}{g}\int_{900\,hPa}^{300\,hPa} V q\, dp \tag{A1}$$

where V is the meridional wind, q is the water vapor mixing ratio, and dp is the pressure level increment. NB: Wille et al. (2019) apply a $-\frac{1}{g}$ factor, with g the gravity acceleration, for dimensional purposes. We do not apply this scaling factor in our detection because we are not interested in vIqT absolute values but only relative to the P97 threshold (which is not affected by a constant multiplicative factor) .

Only poleward fluxes (i.e. V positive in the northern hemisphere, and V negative in the southern hemisphere) are considered. The threshold on $\mathrm{v}IqT_{\mathrm{Wille}}$ is defined as the 98^{th} percentile of $\mathrm{v}IqT_{\mathrm{Wille}}$ (P98), computed for each month and each grid cell, over the 1980–2018 climatology. At each time step, if $\mathrm{v}IqT_{\mathrm{Wille}}$ in a grid cell is above the corresponding month's threshold, the grid cell is counted as an AR-participating point. When an area of continuous AR-participating points is longer than 20 ° latitude, an AR is detected.

In this work, the detection algorithm differs from Wille et al. (2019) as follows. (1) While Wille et al. (2019) keep the original MERRA2 resolution of 0.5 ° lat x 0.625 ° lon, our data is regridded to a 1 °x1 ° spatial resolution. We perform this regridding for data storage management and because we foresee applications of our algorithm for global climate models, which tend to have a resolution closer to 1 °x1 °, (2) instead of limiting the integral between 900 hPa and 300 hPa, the flux is taken for the whole column, in order to leverage the integrated variables provided by MERRA2. This can have an impact over land near the surface where katabatic winds may affect the flux (Wille et al., 2019). As a result, our criterion variable becomes vIxT as described by Equation 1. This vIxT is a pre-computed quantity provided by MERRA2 as an integrated meridional flux. (3) As a result of the two previous differences, our threshold is taken as the P97 of vIxT instead of P98, in order to obtain similar climatologies as in Wille et al. (2019) as shown in Figure A10. (4) The climatology is updated and covers the period 1980–2022.

Our methodology for AR detection is slightly different from the Wille et al. (2019) algorithm, both in terms of input data, detection threshold, and implementation. Therefore a validation is carried out, comparing our results in terms of AR climatology and trends with those from the Wille et al. (2019) catalog. The detection catalog from (Wille et al., 2019) covers the years 1980–2022 and is available through the ARTMIP database `https://doi.org/10.5065/D62R3QFS` (Rutz et al., 2019).

Figure A10 summarizes this comparison, with Figure A10a showing that, for the years 1980–2022, both methodologies yield similar magnitudes and spatial patterns in the frequency of AR detection both in the Arctic and the Antarctic, except for slightly stronger gradients in our detection. In the Arctic, maximum frequencies of around 1% are obtained over Greenland, coming from the Northwest Atlantic region, and in the Bering strait region, coming from the North Pacific, with an additional pathway over Western Russia. In the Antarctic, West Antarctica and the peninsula, along with Queen Maud Land feature a 1% maximum frequency detection in both catalogs. Furthermore, the underlying seasonality of ARs, aggregated by pole (50–80 °N for the Arctic, 50–80 °S for the Antarctic), is the same with both approaches, as described in Figure A10b, with monthly Pearson correlation coefficients of 0.99 and 0.96, for the Arctic and Antarctic, respectively, for the period 1980–2022. This seasonality is stronger in the Arctic with a max-

imum of detection in winter and a minimum in summer. A weaker seasonality with a maximum in austral winter is observed for the Antarctic.

In terms of trends, Figure A10c shows almost identical spatial patterns between the two catalogs. Both catalogs mainly show increasing trends in the regions where AR detection is climatologically most frequent, suggesting an amplification effect more than a change in physical processes. In the Arctic, the Bering strait region features the largest increasing trend with around 1 more AR day per decade. In the Antarctic, West Antarctica and Queen Maud land are the regions where this increasing trend is the most significant with also 1 more AR day per decade. Finally, Figure A10d describes this trend comparison in terms of regionally aggregated time series, showing very similar annual variations along with identical overall increasing trends over the 1980–2022 period.

In conclusion, despite slight methodological differences, the results given by our adapted polar AR detection scheme are very comparable to (Wille et al., 2019), and our detection leveraging vertically integrated variables provided by MERRA2 is therefore fit for purpose and can be duplicated to aerosols.

Another parameter than the threshold percentile that could be tuned for AeRs is the shape criterion imposing a minimum 20 ° extent in latitude. Aerosol sources, including anthropogenic activities and biomass burning, exist in North America and Siberia around 65 °–70 °N. Because of the 20 °-latitude length criterion, AeRs originating from these sources will not be accounted for unless they reach the pole. From an aerosol transport perspective this may seem like a limitation. However, we argue that, by design, AeRs should generally detect extreme, long-range transport of background aerosols from the mid-latitudes, rather than relating to aerosol sources activity. In this respect, we believe it is relevant to keep the 20 °-latitude length condition for aerosols as well, despite the implied rejection of high latitude sources that can be important for the Arctic aerosol budget. For the Antarctic, this criterion is not a problem since all aerosol sources (except sea salt) are further away than 20 ° in latitude.

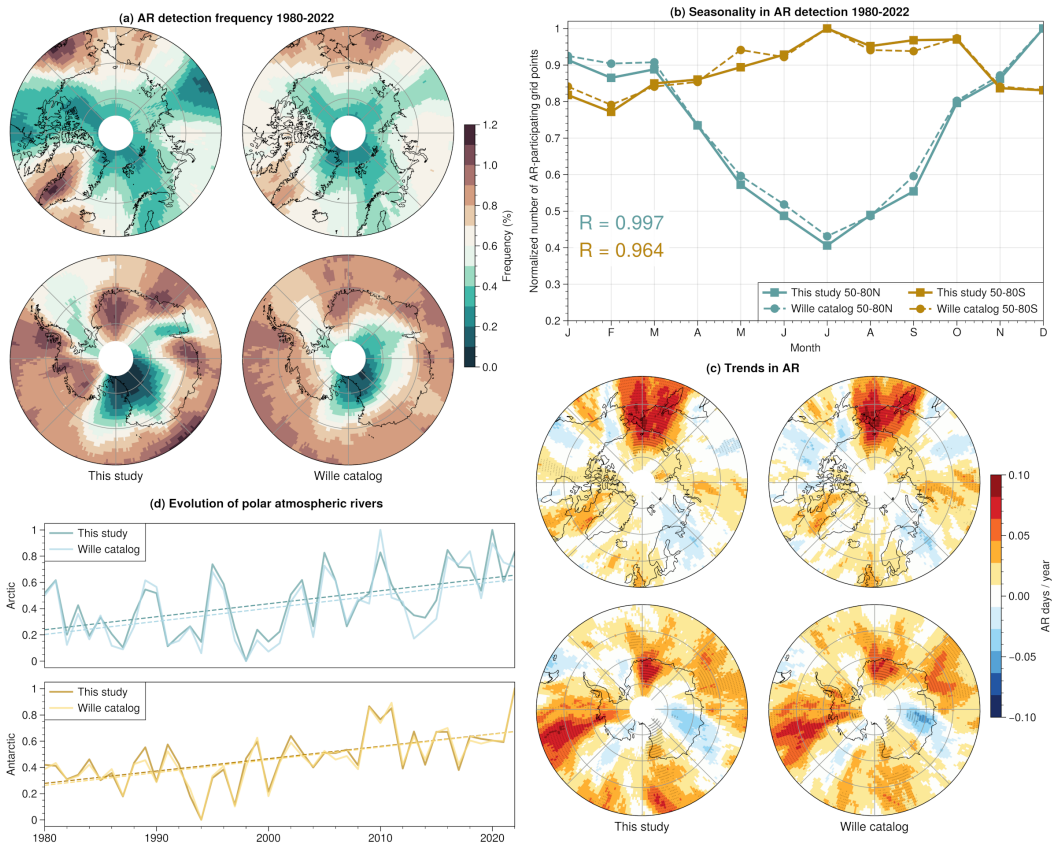

Figure A10. Validation of the adaptations made to the Wille et al. (2019) AR detection scheme. (a) Frequency of AR grid points detected in 1980–2022 using our method (left) and the Wille et al. (2019) method (right). (b) Seasonality in the normalized number of AR grid points in 1980–2022 above 50 ° N (blue) and below 50 ° S (gold), with our method (solid line) and the Wille et al. (2019) method (dashed line). Spatial averaging is weighted by the cell surface. R indicates the Pearson correlation coefficient between our catalog and the Wille et al. (2019) catalog. (c) Trends in AR days per year in the Antarctic, over the period 1980–2022, in this work (left) and in Wille et al. (2021) (right). (d) Relative evolution of AR frequency in the Arctic (top - 50–80 ° N) and Antarctic (bottom - 50–80 ° S) in both catalogs, for the period 1980–2022.

References

Abbatt, J. P. D., Leaitch, W. R., Aliabadi, A. A., Bertram, A. K., Blanchet, J.-P., Boivin-Rioux, A., ... Yakobi-Hancock, J. D. (2019). Overview paper: New insights into aerosol and climate in the Arctic. *Atmospheric Chemistry and Physics*, *19*(4), 2527–2560. doi: 10.5194/acp-19-2527-2019

Adusumilli, S., A. Fish, M., Fricker, H. A., & Medley, B. (2021). Atmospheric River Precipitation Contributed to Rapid Increases in Surface Height of the West Antarctic Ice Sheet in 2019. *Geophysical Research Letters*, *48*(5), e2020GL091076. doi: 10.1029/2020GL091076

Amino, T., Iizuka, Y., Matoba, S., Shimada, R., Oshima, N., Suzuki, T., ... Fujita, K. (2021). Increasing dust emission from ice free terrain in southeastern Greenland since 2000. *Polar Science*, *27*, 100599. doi: 10.1016/j.polar.2020.100599

Barrie, L. A. (1986). Arctic air pollution: An overview of current knowledge. *Atmospheric Environment*, *20*(4), 643–663. doi: 10.1016/0004-6981(86)90180-0

Bintanja, R., van der Wiel, K., van der Linden, E. C., Reusen, J., Bogerd, L., Krikken, F., & Selten, F. M. (2020). Strong future increases in Arctic precipitation variability linked to poleward moisture transport. *Science Advances*, *6*(7), eaax6869. doi: 10.1126/sciadv.aax6869

Bond, T. C., Doherty, S. J., Fahey, D. W., Forster, P. M., Berntsen, T., DeAngelo, B. J., ... Zender, C. S. (2013). Bounding the role of black carbon in the climate system: A scientific assessment. *J. Geophys. Res. Atmos.*, *118*, 5380-5552. doi: 10.1002/jgrd.50171

Boyer, M., Aliaga, D., Pernov, J. B., Angot, H., Quéléver, L. L. J., Dada, L., ... Jokinen, T. (2023). A full year of aerosol size distribution data from the central Arctic under an extreme positive Arctic Oscillation: insights from the Multidisciplinary drifting Observatory for the Study of Arctic Climate (MOSAiC) expedition. *Atmospheric Chemistry and Physics*, *23*(1), 389–415. doi: 10.5194/acp-23-389-2023

Bradski, G. (2000). The OpenCV Library. *Dr. Dobb's Journal of Software Tools*.

Buizert, C., Gkinis, V., Severinghaus, J. P., He, F., Lecavalier, B. S., Kindler, P., ... Brook, E. J. (2014). Greenland temperature response to climate forcing during the last deglaciation. *Science*, *345*(6201), 1177–1180. doi: 10.1126/science.1254961

Bullard, J. E., Baddock, M., Bradwell, T., Crusius, J., Darlington, E., Gaiero, D., ... Thorsteinsson, T. (2016). High-latitude dust in the Earth system. *Reviews of Geophysics*, *54*(2), 447–485. doi: 10.1002/2016RG000518

Böö, S., Ekman, A. M. L., Svensson, G., & Devasthale, A. (2023). Transport of mineral dust into the Arctic in two reanalysis datasets of atmospheric composition. *Tellus B: Chemical and Physical Meteorology*, accepted.

Casado, M., Landais, A., Picard, G., Münch, T., Laepple, T., Stenni, B., ... Jouzel, J. (2018). Archival processes of the water stable isotope signal in East Antarctic ice cores. *The Cryosphere*, *12*(5), 1745–1766. doi: 10.5194/tc-12-1745-2018

Cauquoin, A., Werner, M., & Lohmann, G. (2019). Water isotopes – climate relationships for the mid-Holocene and preindustrial period simulated with an isotope-enabled version of MPI-ESM. *Climate of the Past*, *15*(6), 1913–1937. doi: 10.5194/cp-15-1913-2019

Chakraborty, S., Guan, B., Waliser, D. E., & da Silva, A. M. (2022). Aerosol atmospheric rivers: climatology, event characteristics, and detection algorithm sensitivities. *Atmospheric Chemistry and Physics*, *22*(12), 8175–8195. doi: 10.5194/acp-22-8175-2022

Chakraborty, S., Guan, B., Waliser, D. E., da Silva, A. M., Uluatam, S., & Hess, P. (2021). Extending the atmospheric river concept to aerosols: Climate and air quality impacts. *Geophysical Research Letters*, *48*(9), e2020GL091827. doi:

10.1029/2020GL091827

Chin, M., Ginoux, P., Kinne, S., Torres, O., Holben, B. N., Duncan, B. N., ... Nakajima, T. (2002). Tropospheric Aerosol Optical Thickness from the GOCART Model and Comparisons with Satellite and Sun Photometer Measurements. *Journal of the Atmospheric Sciences*, *59*(3), 461–483. doi: 10.1175/1520-0469(2002)059⟨0461:TAOTFT⟩2.0.CO;2

Clem, K. R., Bozkurt, D., Kennett, D., King, J. C., & Turner, J. (2022). Central tropical Pacific convection drives extreme high temperatures and surface melt on the Larsen C Ice Shelf, Antarctic Peninsula. *Nature Communications*, *13*(1), 3906. doi: 10.1038/s41467-022-31119-4

Collow, A. B. M., Shields, C. A., Guan, B., Kim, S., Lora, J. M., McClenny, E. E., ... Wehner, M. (2022). An Overview of ARTMIP's Tier 2 Reanalysis Intercomparison: Uncertainty in the Detection of Atmospheric Rivers and Their Associated Precipitation. *Journal of Geophysical Research: Atmospheres*, *127*(8), e2021JD036155. doi: 10.1029/2021JD036155

Corbett, J. J., Lack, D. A., Winebrake, J. J., Harder, S., Silberman, J. A., & Gold, M. (2010). Arctic shipping emissions inventories and future scenarios. *Atmospheric Chemistry and Physics*, *10*(19), 9689–9704. doi: 10.5194/acp-10-9689-2010

Creamean, J. M., Suski, K. J., Rosenfeld, D., Cazorla, A., DeMott, P. J., Sullivan, R. C., ... Prather, K. A. (2013). Dust and Biological Aerosols from the Sahara and Asia Influence Precipitation in the Western U.S. *Science*, *339*(6127), 1572–1578. doi: 10.1126/science.1227279

Dada, L., Angot, H., Beck, I., Baccarini, A., Quéléver, L. L. J., Boyer, M., ... Schmale, J. (2022). A central arctic extreme aerosol event triggered by a warm air-mass intrusion. *Nature Communications*, *13*(1), 1–15. doi: 10.1038/s41467-022-32872-2

Eastman, R., & Warren, S. G. (2010). Interannual Variations of Arctic Cloud Types in Relation to Sea Ice. *Journal of Climate*, *23*, 4216–4232. doi: 10.1175/2010JCLI3492.1

Francis, D., Fonseca, R., Nelli, N., Bozkurt, D., Picard, G., & Guan, B. (2022). Atmospheric rivers drive exceptional Saharan dust transport towards Europe. *Atmospheric Research*, *266*, 105959. doi: 10.1016/j.atmosres.2021.105959

Frey, M. M., Norris, S. J., Brooks, I. M., Anderson, P. S., Nishimura, K., Yang, X., ... Wolff, E. W. (2020). First direct observation of sea salt aerosol production from blowing snow above sea ice. *Atmospheric Chemistry and Physics*, *20*, 2549–2578. doi: 10.5194/acp-20-2549-2020

Gershunov, A., Shulgina, T., Ralph, F. M., Lavers, D. A., & Rutz, J. J. (2017). Assessing the climate-scale variability of atmospheric rivers affecting western north america. *Geophysical Research Letters*, *44*(15), 7900-7908. doi: 10.1002/2017GL074175

Global Modeling and Assimilation Office (GMAO). (2015a). *MERRA-2 inst3_3d_aer_Nv: 3d,3-Hourly,Instantaneous,Model-Level,Assimilation,Aerosol Mixing Ratio V5.12.4 [Dataset].* Goddard Earth Sciences Data and Information Services Center (GES DISC). (last accessed: April 15, 2023) doi: 10.5067/LTVB4GPCOTK2

Global Modeling and Assimilation Office (GMAO). (2015b). *MERRA-2 tavg1_2d_aer_Nx: 2d,1-Hourly,Time-averaged,Single-Level,Assimilation,Aerosol Diagnostics V5.12.4 [Dataset].* Goddard Earth Sciences Data and Information Services Center (GES DISC). (last accessed: April 15, 2023) doi: 10.5067/KLICLTZ8EM9D

Global Modeling and Assimilation Office (GMAO). (2015c). *MERRA-2 tavg1_2d_int_Nx: 2d,1-Hourly,Time-Averaged,Single-Level,Assimilation,Vertically Integrated Diagnostics V5.12.4 [Dataset].* Goddard Earth Sciences Data and Information Services Center (GES DISC). (last

accessed: April 15, 2023) doi: 10.5067/Q5GVUVUIVGO7

Global Modeling and Assimilation Office (GMAO). (2015d). *MERRA-2 tavg1_2d_slv_Nx: 2d,1-Hourly,Time-Averaged,Single-Level,Assimilation,Single-Level Diagnostics V5.12.4 [Dataset].* Goddard Earth Sciences Data and Information Services Center (GES DISC). (last accessed: April 15, 2023) doi: 10.5067/VJAFPLI1CSIV

Global Modeling and Assimilation Office (GMAO). (2015e). *MERRA-2 tavgM_2d_adg_Nx: 2d,Monthly mean,Time-averaged,Single-Level,Assimilation,Aerosol Diagnostics (extended) V5.12.4 [Dataset].* Goddard Earth Sciences Data and Information Services Center (GES DISC). (last accessed: April 15, 2023) doi: 10.5067/RZIK2TV7PP38

Gorodetskaya, I., Tsukernik, M., Claes, K., Ralph, M. F., Neff, W. D., & Van Lipzig, N. P. M. (2014). The role of atmospheric rivers in anomalous snow accumulation in east antarctica. *Geophysical Research Letters*, *41*(17), 6199-6206. doi: https://doi.org/10.1002/2014GL060881

Goursaud, S., Masson-Delmotte, V., Favier, V., Preunkert, S., Legrand, M., Minster, B., & Werner, M. (2019). Challenges associated with the climatic interpretation of water stable isotope records from a highly resolved firn core from Adélie Land, coastal Antarctica. *The Cryosphere*, *13*(4), 1297–1324. doi: 10.5194/tc-13-1297-2019

Hall, A. (2004). The Role of Surface Albedo Feedback in Climate. *Journal of Climate*, *17*, 1550–1568. doi: 10.1175/1520-0442(2004)017⟨1550:TROSAF⟩2.0.CO;2

Held, I. M., & Soden, B. J. (2006). Robust Responses of the Hydrological Cycle to Global Warming. *Journal of Climate*, *19*(21), 5686–5699. doi: 10.1175/JCLI3990.1

Heutte, B., Beck, I., Quéléver, L., Jokinen, T., Laurila, T., Dada, L., & Schmale, J. (2022). *Equivalent black carbon concentration in 10 minutes time resolution, measured in the Swiss container during MOSAiC 2019/2020 [dataset].* PANGAEA. doi: 10.1594/PANGAEA.952251

Hunter, J. D. (2007). Matplotlib: A 2d graphics environment. *Computing in Science & Engineering*, *9*(3), 90–95. doi: 10.1109/MCSE.2007.55

Jouzel, J., Alley, R. B., Cuffey, K. M., Dansgaard, W., Grootes, P., Hoffmann, G., ... White, J. (1997). Validity of the temperature reconstruction from water isotopes in ice cores. *Journal of Geophysical Research: Oceans*, *102*(C12), 26471-26487. doi: https://doi.org/10.1029/97JC01283

Jumelet, J., Klekociuk, A. R., Alexander, S. P., Bekki, S., Hauchecorne, A., Vernier, J. P., ... Keckhut, P. (2020). Detection of Aerosols in Antarctica From Long-Range Transport of the 2009 Australian Wildfires. *Journal of Geophysical Research: Atmospheres*, *125*(23), e2020JD032542. doi: 10.1029/2020JD032542

Kirpes, R. M., Bonanno, D., May, N. W., Fraund, M., Barget, A. J., Moffet, R. C., ... Pratt, K. A. (2019). Wintertime Arctic Sea Spray Aerosol Composition Controlled by Sea Ice Lead Microbiology. *ACS Cent. Sci.*, *5*, 1760–1767. doi: 10.1021/acscentsci.9b00541

Kluyver, T., Ragan-Kelley, B., Pérez, F., Granger, B., Bussonnier, M., Frederic, J., ... Willing, C. (2016). Jupyter notebooks – a publishing format for reproducible computational workflows. In F. Loizides & B. Schmidt (Eds.), *Positioning and power in academic publishing: Players, agents and agendas* (p. 87 - 90).

Komatsu, K. K., Alexeev, V. A., Repina, I. A., & Tachibana, Y. (2018). Poleward upgliding Siberian atmospheric rivers over sea ice heat up Arctic upper air. *Scientific Reports*, *8*(1), 2872. doi: 10.1038/s41598-018-21159-6

Krinner, G., & Genthon, C. (2003). Tropospheric transport of continental tracers towards Antarctica under varying climatic conditions. *Tellus B*, *55*(1), 54–70. doi: 10.1034/j.1600-0889.2003.00004.x

Krinner, G., & Werner, M. (2003). Impact of precipitation seasonality changes on isotopic signals in polar ice cores: a multi-model analysis. *Earth and Planetary Science Letters*, *216*(4), 525–538. doi: 10.1016/S0012-821X(03)00550-8

Lachlan-Cope, T. (2010). Antarctic clouds. *Polar Research*, *29*, 150–158. doi: 10.3402/polar.v29i2.6065

Lapere, R. (2023, June). *Polar atmospheric and aerosol river detection catalogs [Dataset/Software].* Zenodo. doi: 10.5281/zenodo.8082768

Lapere, R., Thomas, J. L., Marelle, L., Ekman, A. M. L., Frey, M. M., Lund, M. T., ... Zieger, P. (2023). The Representation of Sea Salt Aerosols and Their Role in Polar Climate Within CMIP6. *Journal of Geophysical Research: Atmospheres*, *128*(6), e2022JD038235. doi: 10.1029/2022JD038235

Lavers, D. A., Villarini, G., Allan, R. P., Wood, E. F., & Wade, A. J. (2012). The detection of atmospheric rivers in atmospheric reanalyses and their links to British winter floods and the large-scale climatic circulation. *Journal of Geophysical Research: Atmospheres*, *117*, D20. doi: 10.1029/2012JD018027

Levine, J. G., Yang, X., Jones, A. E., & Wolff, E. W. (2014). Sea salt as an ice core proxy for past sea ice extent: A process-based model study. *Journal of Geophysical Research: Atmospheres*, *119*(9), 5737–5756. doi: 10.1002/2013JD020925

Maclennan, M. L., & Lenaerts, J. T. M. (2021). Large-scale atmospheric drivers of snowfall over thwaites glacier, antarctica. *Geophysical Research Letters*, *48*(17), e2021GL093644. doi: https://doi.org/10.1029/2021GL093644

Maclennan, M. L., Lenaerts, J. T. M., Shields, C. A., Hoffman, A. O., Wever, N., Thompson-Munson, M., ... Wille, J. D. (2023). Climatology and surface impacts of atmospheric rivers on West Antarctica. *The Cryosphere*, *17*(2), 865–881. doi: 10.5194/tc-17-865-2023

Marelle, L., Raut, J.-C., Law, K. S., & Duclaux, O. (2018). Current and Future Arctic Aerosols and Ozone From Remote Emissions and Emerging Local Sources—Modeled Source Contributions and Radiative Effects. *Journal of Geophysical Research: Atmospheres*, *123*(22), 12,942–12,963. doi: 10.1029/2018JD028863

Mattingly, K. S., Mote, T. L., & Fettweis, X. (2018). Atmospheric River Impacts on Greenland Ice Sheet Surface Mass Balance. *Journal of Geophysical Research: Atmospheres*, *123*(16), 8538–8560. doi: 10.1029/2018JD028714

Matus, A. V., & L'Ecuyer, T. S. (2017). The role of cloud phase in Earth's radiation budget. *Journal of Geophysical Research: Atmospheres*, *122*(5), 2559–2578. doi: 10.1002/2016JD025951

Mei, L., Xue, Y., de Leeuw, G., von Hoyningen-Huene, W., Kokhanovsky, A. A., Istomina, L., ... Burrows, J. P. (2013). Aerosol optical depth retrieval in the Arctic region using MODIS data over snow. *Remote Sensing of Environment*, *128*, 234–245. doi: 10.1016/j.rse.2012.10.009

Meinander, O., Dagsson-Waldhauserova, P., Amosov, P., Aseyeva, E., Atkins, C., Baklanov, A., ... Vukovic Vimic, A. (2022). Newly identified climatically and environmentally significant high-latitude dust sources. *Atmospheric Chemistry and Physics*, *22*(17), 11889–11930. doi: 10.5194/acp-22-11889-2022

Murray, B. J., Carslaw, K. S., & Field, P. R. (2021). Opinion: Cloud-phase climate feedback and the importance of ice-nucleating particles. *Atmospheric Chemistry and Physics*, *21*(2), 665–679. doi: 10.5194/acp-21-665-2021

Murray, B. J., O'Sullivan, D., Atkinson, J. D., & Webb, M. E. (2012). Ice nucleation by particles immersed in supercooled cloud droplets. *Chemical Society Reviews*, *41*(19), 6519–6554. doi: 10.1039/C2CS35200A

Myhre, G., Shindell, D., Bréon, F.-M., Collins, W., Fuglestvedt, J., Huang, J., ... Zhang, H. (2013). Climate Change 2013: The Physical Science Basis. Contribution of Working Group I to the Fifth Assessment Report of the Intergovernmental Panel on Climate Change [Stocker, T.F., D. Qin, G.-K. Plattner, M.

Tignor, S.K. Allen, J. Boschung, A. Nauels, Y. Xia, V. Bex and P.M. Midgley (eds.)]. In (chap. Anthropogenic and Natural Radiative Forcing). Cambridge University Press, Cambridge, UK and New York, NY, USA.

NASA. (2013). *EOSDIS Worldview.* Retrieved from `https://worldview.earthdata.nasa.gov/`

Nash, D., Waliser, D., Guan, B., Ye, H., & Ralph, F. M. (2018). The Role of Atmospheric Rivers in Extratropical and Polar Hydroclimate. *Journal of Geophysical Research: Atmospheres*, *123*(13), 6804–6821. doi: 10.1029/2017JD028130

Neiman, P. J., Ralph, F. M., Moore, B. J., Hughes, M., Mahoney, K. M., Cordeira, J. M., & Dettinger, M. D. (2013). The Landfall and Inland Penetration of a Flood-Producing Atmospheric River in Arizona. Part I: Observed Synoptic-Scale, Orographic, and Hydrometeorological Characteristics. *Journal of Hydrometeorology*, *14*(2), 460–484. doi: 10.1175/JHM-D-12-0101.1

Nygård, T., Naakka, T., & Vihma, T. (2020). Horizontal Moisture Transport Dominates the Regional Moistening Patterns in the Arctic. *Journal of Climate*, *33*(16), 6793–6807. doi: 10.1175/JCLI-D-19-0891.1

O'Brien, T. A., Wehner, M. F., Payne, A. E., Shields, C. A., Rutz, J. J., Leung, L.-R., ... Zhou, Y. (2022). Increases in Future AR Count and Size: Overview of the ARTMIP Tier 2 CMIP5/6 Experiment. *Journal of Geophysical Research: Atmospheres*, *127*(6), e2021JD036013. doi: 10.1029/2021JD036013

Papritz, L., Hauswirth, D., & Hartmuth, K. (2022). Moisture origin, transport pathways, and driving processes of intense wintertime moisture transport into the Arctic. *Weather and Climate Dynamics*, *3*, 1–20. doi: 10.5194/wcd-3-1-2022

Pernov, J. B., Beddows, D., Thomas, D. C., Dall´Osto, M., Harrison, R. M., Schmale, J., ... Massling, A. (2022). Increased aerosol concentrations in the High Arctic attributable to changing atmospheric transport patterns. *npj Climate and Atmospheric Science*, *5*(1), 1–13. doi: 10.1038/s41612-022-00286-y

Pithan, F., Svensson, G., Caballero, R., Chechin, D., Cronin, T. W., Ekman, A. M. L., ... Wendisch, M. (2018). Role of air-mass transformations in exchange between the Arctic and mid-latitudes. *Nature Geoscience*, *11*(11), 805–812. doi: 10.1038/s41561-018-0234-1

Pohl, B., Favier, V., Wille, J., Udy, D. G., Vance, T. R., Pergaud, J., ... Codron, F. (2021). Relationship Between Weather Regimes and Atmospheric Rivers in East Antarctica. *Journal of Geophysical Research: Atmospheres*, *126*(24), e2021JD035294. doi: 10.1029/2021JD035294

Quinn, P. K., Shaw, G., Andrews, E., Dutton, E. G., Ruoho-Airola, T., & Gong, S. L. (2007). Arctic haze: current trends and knowledge gaps. *Tellus B*, *59*, 99–114. doi: 10.1111/j.1600-0889.2006.00238.x

Ralph, F. M., Rutz, J. J., Cordeira, J. M., Dettinger, M., Anderson, M., Reynolds, D., ... Smallcomb, C. (2019). A Scale to Characterize the Strength and Impacts of Atmospheric Rivers. *Bulletin of the American Meteorological Society*, *100*(2), 269–289. doi: 10.1175/BAMS-D-18-0023.1

Rantanen, M., Karpechko, A. Y., Lipponen, A., Nordling, K., Hyvärinen, O., Ruosteenoja, K., ... Laaksonen, A. (2022). The Arctic has warmed nearly four times faster than the globe since 1979. *Commun Earth Environ*, *3*, 1–10. doi: 10.1038/s43247-022-00498-3

Raut, J.-C., Marelle, L., Fast, J. D., Thomas, J. L., Weinzierl, B., Law, K. S., ... Schlager, H. (2017). Cross-polar transport and scavenging of Siberian aerosols containing black carbon during the 2012 ACCESS summer campaign. *Atmospheric Chemistry and Physics*, *17*(18), 10969–10995. doi: 10.5194/acp-17-10969-2017

Rhodes, R. H., Yang, X., & Wolff, E. W. (2018). Sea Ice Versus Storms: What Controls Sea Salt in Arctic Ice Cores? *Geophysical Research Letters*, *45*(11), 5572–5580. doi: 10.1029/2018GL077403

Rinke, A., Segger, B., Crewell, S., Maturilli, M., Naakka, T., Nygård, T., ... Keller,

J. (2019). Trends of Vertically Integrated Water Vapor over the Arctic during 1979–2016: Consistent Moistening All Over? *Journal of Climate*, *32*(18), 6097–6116. doi: 10.1175/JCLI-D-19-0092.1

Roiger, A., Schlager, H., Schäfler, A., Huntrieser, H., Scheibe, M., Aufmhoff, H., ... Arnold, F. (2011). In-situ observation of Asian pollution transported into the Arctic lowermost stratosphere. *Atmospheric Chemistry and Physics*, *11*(21), 10975–10994. doi: 10.5194/acp-11-10975-2011

Rutz, J. J., Shields, C. A., Lora, J. M., Payne, A. E., Guan, B., Ullrich, P. A., ... Viale, M. (2019). *Artmip tier-1 catalogues, ucar [dataset].* (Last access date: 20 April 2023) doi: 10.5065/D62R3QFS

Schmale, J., Zieger, P., & Ekman, A. M. L. (2021). Aerosols in current and future Arctic climate. *Nature Climate Change*, *11*(2), 95–105. doi: 10.1038/s41558-020-00969-5

Servettaz, A. P. M., Orsi, A. J., Curran, M. A. J., Moy, A. D., Landais, A., McConnell, J. R., ... Chappellaz, J. (2023). A 2000-year temperature reconstruction on the East Antarctic plateau from argon–nitrogen and water stable isotopes in the Aurora Basin North ice core. *Climate of the Past*, *19*(6), 1125–1152. doi: 10.5194/cp-19-1125-2023

Shi, Y., Liu, X., Wu, M., Zhao, X., Ke, Z., & Brown, H. (2022). Relative importance of high-latitude local and long-range-transported dust for Arctic ice-nucleating particles and impacts on Arctic mixed-phase clouds. *Atmospheric Chemistry and Physics*, *22*(4), 2909–2935. doi: 10.5194/acp-22-2909-2022

Shields, C. A., Payne, A. E., Shearer, E. J., Wehner, M. F., O'Brien, T. A., Rutz, J. J., ... Zarzycki, C. (2023). Future Atmospheric Rivers and Impacts on Precipitation: Overview of the ARTMIP Tier 2 High-Resolution Global Warming Experiment. *Geophysical Research Letters*, *50*(6), e2022GL102091. doi: 10.1029/2022GL102091

Shields, C. A., Rosenbloom, N., Bates, S., Hannay, C., Hu, A., Payne, A. E., ... Truesdale, J. (2019). Meridional Heat Transport During Atmospheric Rivers in High-Resolution CESM Climate Projections. *Geophysical Research Letters*, *46*(24), 14702–14712. doi: 10.1029/2019GL085565

Shields, C. A., Rutz, J. J., Leung, L.-Y., Ralph, F. M., Wehner, M., Kawzenuk, B., ... Nguyen, P. (2018). Atmospheric River Tracking Method Intercomparison Project (ARTMIP): project goals and experimental design. *Geoscientific Model Development*, *11*(6), 2455–2474. doi: 10.5194/gmd-11-2455-2018

Shields, C. A., Wille, J. D., Marquardt Collow, A. B., Maclennan, M., & Gorodetskaya, I. V. (2022). Evaluating Uncertainty and Modes of Variability for Antarctic Atmospheric Rivers. *Geophysical Research Letters*, *49*(16), e2022GL099577. doi: 10.1029/2022GL099577

Shupe, M. D., Rex, M., Blomquist, B., Persson, P. O. G., Schmale, J., Uttal, T., ... Yue, F. (2022). Overview of the MOSAiC expedition: Atmosphere. *Elementa: Science of the Anthropocene*, *10*(1), 00060. doi: 10.1525/elementa.2021.00060

Skiles, S. M., Flanner, M., Cook, J. M., Dumont, M., & Painter, T. H. (2018). Radiative forcing by light-absorbing particles in snow. *Nature Climate Change*, *8*(11), 964–971. doi: 10.1038/s41558-018-0296-5

Sodemann, H., Pommier, M., Arnold, S. R., Monks, S. A., Stebel, K., Burkhart, J. F., ... Stohl, A. (2011). Episodes of cross-polar transport in the Arctic troposphere during July 2008 as seen from models, satellite, and aircraft observations. *Atmospheric Chemistry and Physics*, *11*(8), 3631–3651. doi: 10.5194/acp-11-3631-2011

Stohl, A. (2006). Characteristics of atmospheric transport into the Arctic troposphere. *Journal of Geophysical Research: Atmospheres*, *111*. doi: 10.1029/2005JD006888

Szopa, S., Naik, V., Adhikary, B., Artaxo, P., Berntsen, T., Collins, W., ... Zanis, P. (2021). Climate Change 2021: The Physical Science Basis. Contribution

of Working Group I to the Sixth Assessment Report of the Intergovernmental Panel on Climate Change [Masson-Delmotte, V., P. Zhai, A. Pirani, S.L. Connors, C. Pean, S. Berger, N. Caud, Y. Chen, L. Goldfarb, M.I. Gomis, M. Huang, K. Leitzell, E. Lonnoy, J.B.R. Matthews, T.K. Maycock, T. Waterfield, O. Yelekci, R. Yu, and B. Zhou (eds.)]. In (chap. Short-Lived Climate Forcers). Cambridge University Press, Cambridge, United Kingdom and New York, NY, USA. doi: 10.1017/9781009157896.008

Tan, I., & Storelvmo, T. (2019). Evidence of Strong Contributions From Mixed-Phase Clouds to Arctic Climate Change. *Geophysical Research Letters*, *46*(5), 2894–2902. doi: 10.1029/2018GL081871

Thomas, J. L., Polashenski, C. M., Soja, A. J., Marelle, L., Casey, K. A., Choi, H. D., ... Dibb, J. E. (2017). Quantifying black carbon deposition over the Greenland ice sheet from forest fires in Canada. *Geophysical Research Letters*, *44*(15), 7965–7974. doi: 10.1002/2017GL073701

Thomas, M. A., Devasthale, A., Tjernström, M., & Ekman, A. M. L. (2019). The Relation Between Aerosol Vertical Distribution and Temperature Inversions in the Arctic in Winter and Spring. *Geophysical Research Letters*, *46*(5), 2836–2845. doi: 10.1029/2018GL081624

Turner, J., Phillips, T., Hosking, J. S., Marshall, G. J., & Orr, A. (2013). The Amundsen Sea low. *International Journal of Climatology*, *33*(7), 1818–1829. doi: 10.1002/joc.3558

Turner, J., Phillips, T., Thamban, M., Rahaman, W., Marshall, G. J., Wille, J. D., ... Lachlan-Cope, T. (2019). The Dominant Role of Extreme Precipitation Events in Antarctic Snowfall Variability. *Geophysical Research Letters*, *46*(6), 3502–3511. doi: 10.1029/2018GL081517

Wahl, S., Steen-Larsen, H. C., Hughes, A. G., Dietrich, L. J., Zuhr, A., Behrens, M., ... Hörhold, M. (2022). Atmosphere-Snow Exchange Explains Surface Snow Isotope Variability. *Geophysical Research Letters*, *49*(20), e2022GL099529. doi: 10.1029/2022GL099529

Wendisch, M., Brückner, M., Crewell, S., Ehrlich, A., Notholt, J., Lüpkes, C., ... Rinke, e. a., A. (2023). Atmospheric and Surface Processes, and Feedback Mechanisms Determining Arctic Amplification: A Review of First Results and Prospects of the (AC)3 Project. *Bulletin of the American Meteorological Society*, *104*(1), E208–E242. doi: 10.1175/BAMS-D-21-0218.1

Werner, M., Heimann, M., & Hoffmann, G. (2001). Isotopic composition and origin of polar precipitation in present and glacial climate simulations. *Tellus B: Chemical and Physical Meteorology*, *53*(1), 53–71. doi: 10.3402/tellusb.v53i1.16539

Wille, J. D., Favier, V., Dufour, A., Gorodetskaya, I. V., Turner, J., Agosta, C., & Codron, F. (2019). West Antarctic surface melt triggered by atmospheric rivers. *Nature Geoscience*, *12*(11), 911–916. doi: 10.1038/s41561-019-0460-1

Wille, J. D., Favier, V., Gorodetskaya, I. V., Agosta, C., Kittel, C., Beeman, J. C., ... Codron, F. (2021). Antarctic Atmospheric River Climatology and Precipitation Impacts. *Journal of Geophysical Research: Atmospheres*, *126*, e2020JD033788. doi: 10.1029/2020JD033788

Wille, J. D., Favier, V., Jourdain, N. C., Kittel, C., Turton, J. V., Agosta, C., ... Berchet, A. (2022). Intense atmospheric rivers can weaken ice shelf stability at the Antarctic Peninsula. *Communications Earth & Environment*, *3*, 1–14. doi: 10.1038/s43247-022-00422-9

Wolff, E. W., Fischer, H., Fundel, F., Ruth, U., Twarloh, B., Littot, G. C., ... Gaspari, V. (2006). Southern Ocean sea-ice extent, productivity and iron flux over the past eight glacial cycles. *Nature*, *440*(7083), 491–496. doi: 10.1038/nature04614

Xu, J.-W., Martin, R. V., Morrow, A., Sharma, S., Huang, L., Leaitch, W. R., ... Abbatt, J. P. D. (2017). Source attribution of Arctic black carbon constrained

by aircraft and surface measurements. *Atmospheric Chemistry and Physics*, *17*(19), 11971–11989. doi: 10.5194/acp-17-11971-2017

Yang, X., Pyle, J. A., & Cox, R. A. (2008). Sea salt aerosol production and bromine release: Role of snow on sea ice. *Geophysical Research Letters*, *35*, L16815. doi: 10.1029/2008GL034536

You, C., Tjernström, M., Devasthale, A., & Steinfeld, D. (2022). The Role of Atmospheric Blocking in Regulating Arctic Warming. *Geophysical Research Letters*, *49*(12), e2022GL097899. doi: 10.1029/2022GL097899

Zhang, P., Chen, G., Ting, M., Ruby Leung, L., Guan, B., & Li, L. (2023). More frequent atmospheric rivers slow the seasonal recovery of Arctic sea ice. *Nature Climate Change*, *13*(3), 266–273. doi: 10.1038/s41558-023-01599-3

Zhao, X., Huang, K., Fu, J. S., & Abdullaev, S. F. (2022). Long-range transport of Asian dust to the Arctic: identification of transport pathways, evolution of aerosol optical properties, and impact assessment on surface albedo changes. *Atmospheric Chemistry and Physics*, *22*(15), 10389–10407. doi: 10.5194/acp-22-10389-2022

Zhou, Y., Wu, T., Zhou, Y., Zhang, J., Zhang, F., Su, X., ... Wang, J. (2023). Can global warming bring more dust? *Climate Dynamics*. doi: 10.1007/s00382-023-06706-w

Zhu, Y., & Newell, R. E. (1998). A Proposed Algorithm for Moisture Fluxes from Atmospheric Rivers. *Monthly Weather Review*, *126*(3), 725–735. doi: 10.1175/1520-0493(1998)126⟨0725:APAFMF⟩2.0.CO;2